catalysts

MDPI

Article

Support Effect on the Performance of Ni_2P Catalysts in the Hydrodeoxygenation of Methyl Palmitate

Irina V. Deliy *, Ivan V. Shamanaev, Pavel V. Aleksandrov, Evgeny Yu. Gerasimov, Vera P. Pakharukova, Evgeny G. Kodenev, Ilya V. Yakovlev, Olga B. Lapina and Galina A. Bukhtiyarova

Boreskov Institute of Catalysis, Pr. Lavrentieva 5, 630090 Novosibirsk, Russia; i.v.shamanaev@catalysis.ru (I.V.S.); aleksandrov@catalysis.ru (P.V.A.); gerasimov@catalysis.ru (E.Y.G.); verapakharukova@yandex.ru (V.P.P.); kodenev_e@mail.ru (E.G.K.); spitzstichel@gmail.com (I.V.Y.); olga@catalysis.ru (O.B.L.); gab@catalysis.ru (G.A.B.)

* Correspondence: delij@catalysis.ru; Tel.: +7-383-326-9410

Received: 11 October 2018; Accepted: 31 October 2018; Published: 3 November 2018

Abstract: The effect of support nature, SiO_2 and γ-Al_2O_3, on physicochemical and catalytic properties of nickel phosphide catalysts in methyl palmitate hydrodeoxygenation (HDO) has been considered. Firstly, alumina-supported nickel phosphide catalysts prepared by temperature-programmed reduction method starting from different precursors (phosphate–$Ni(NO_3)_2$ and $(NH_4)_2HPO_4$ or phosphite–$Ni(OH)_2$ and H_3PO_3) were compared using elemental analysis, N_2 physisorption, H_2-TPR, XRD, TEM, NH_3-TPD, ^{27}Al and ^{31}P MAS NMR techniques and catalytic experiments. The mixture of nickel phosphide phases was produced from phosphate precursor on alumina while using of phosphite precursor provides Ni_2P formation with the higher activity in methyl palmitate HDO. Besides, the comparative study of the performances of Ni_2P/SiO_2 and Ni_2P/Al_2O_3 catalysts demonstrates the apparent superiority of alumina-supported Ni_2P in the methyl palmitate hydrodeoxygenation. Considering the tentative scheme of methyl palmitate transformation, we proposed that cooperation of Ni_2P and acid sites on the surface of alumina provides the enhanced activity of alumina-supported Ni_2P through the acceleration of acid-catalysed hydrolysis.

Keywords: nickel phosphide; acidity; Ni_2P/γ-Al_2O_3; Ni_2P/SiO_2; methyl palmitate; hydrodeoxygenation; biofuel; green diesel

1. Introduction

Depletion of fossil oils resources, as well as the environmental issues of increased carbon emission, stimulates the development of new catalytic technologies for the production of transportation fuels from renewable [1–3]. Triglyceride-based feedstocks, such as non-edible vegetable oils, animal fats and waste cooking oils, are the attractive resources that give a mixture of C_{14}-C_{18} alkanes in the hydrodeoxygenation (HDO) process [2,4,5]. This product called green diesel has a high cetane number and stability, low density and can be mixed with the fossil-derived fuels to improve their quality [6–8].

Recently, noble metal-based and sulphide hydrotreating catalysts have been studied intensively in the HDO of triglycerides and model compounds, such as aliphatic esters [3–5]. However, the practical application of noble metal catalysts, despite their high HDO activity, is restricted by the high cost and shortage of noble metals. As to hydrotreating sulphide catalysts, the S-containing agent has to be added to the feed to avoid deactivation that, in turn, leads to the appearance of undesirable S-containing products [9–11]. Besides, the catalytic properties of supported noble metals and sulphide phase can be deteriorated by the reaction products–carbon oxides and water [12–14]. Thus, new systems containing base metals or their carbides, nitrides and phosphides have emerged as the catalysts for HDO of

aliphatic esters and vegetable oils in recent years [2–4,15,16]. Among them, silica-supported nickel phosphide catalysts attract the particular attention of researchers due to their high stability and activity in HDO reactions [3,16–28].

Effects of the precursor, initial Ni/P ratio and preparation conditions on the catalytic properties of Ni_xP_y/SiO_2 systems in the HDO of aliphatic esters were studied using mainly methyl oleate [18,20], methyl laurate [15,17,19,28,29] and methyl palmitate [21,24–27]. In most studies, the activity of Ni_xP_y/SiO_2 catalysts was shown to be higher than the activity of Ni/SiO_2 samples and the decrease of Ni/P ratio in the impregnation solution improved the catalytic activity and selectivity towards direct HDO (formation of C_n hydrocarbons through H_2O elimination) [21,24,27]. It was stated that the Ni_2P phase is the most active in hydrodeoxygenation of fatty acid methyl esters among the variety of supported nickel phosphides such as Ni_3P, Ni_2P, Ni_5P_4 and $Ni_{12}P_5$ [17,20,23,27]. The optimal calcination and reduction conditions of Ni_xP_y/SiO_2 precursors for obtaining the most active catalysts in HDO were found [25,26,30].

In our previous study we have found out the synergetic effect of Ni_2P/SiO_2 and γ-Al_2O_3 physical mixture in hydrodeoxygenation of methyl palmitate, which was explained by the cooperation of the metal sites of Ni_2P/SiO_2 and the acid sites of γ-Al_2O_3 in consecutive metal-catalysed and acid-catalysed reactions of methyl palmitate conversion [31]. Therefore, we proposed, that the employment of γ-Al_2O_3 as the support can improve the activity of the Ni_2P catalyst due to the ability of the former to accelerate the aliphatic esters hydrolysis [32,33].

It is well known, that support nature can influence the activity of the catalysts by affecting the active component properties, namely active phase and dispersity, at the stage of catalyst preparation [22,34–37] or as a result of the participation of the support in catalytic conversions [33,35,37–40]. The support effect on the catalytic properties of nickel phosphide catalysts has been studied in the hydrodechlorination of chlorobenzene [41,42], hydrodesulfurization of thiophene [43] and hydrodeoxygenation of guaiacol [44]. Recently, deoxygenation of methyl laurate over nickel phosphide catalysts supported on SiO_2, CeO_2, TiO_2, γ-Al_2O_3 and SAPO-11 was also investigated [22]. However, in this study different nickel phosphide phases were formed depending on the support: Ni_2P was produced on SiO_2, CeO_2, TiO_2 and SAPO-11, while Ni_3P and $Ni_{12}P_5$ were received on γ-Al_2O_3. The authors concluded that the catalyst activity of nickel phosphide catalysts in methyl laurate HDO depends on several factors, namely surface density of Ni sites, the electron property of metal sites, the Ni_2P crystallite size and the synergism between the Ni sites and the acid sites.

The aim of our current study is to elucidate the real support effect, without the interference of other crucial factors, like phase composition, Ni content or Ni_2P particle size through the comparative study of the performance of Ni_2P/SiO_2 and Ni_2P/Al_2O_3 catalysts in the methyl palmitate hydrodeoxygenation. Firstly, the alumina-supported nickel phosphide catalysts differing in the precursor and reduction temperature have been investigated by elemental analysis, N_2 physisorption, H_2-TPR, XRD, TEM, NH_3-TPD, ^{27}Al and ^{31}P MAS NMR. It turned out that the reduction of the phosphite-type precursor at 550–650 °C makes it possible to support Ni_2P nanoparticles on the alumina surface with the particle size distribution resembling that on the surface of Ni_2P/SiO_2 catalysts, obtained in our previous study from phosphide precursor [26]. The comparison of the catalyst's behaviour in the wide temperature interval showed the superior activity of the alumina-supported catalyst in comparison with the silica-supported one. The higher activity of Ni_2P/Al_2O_3 catalyst in methyl palmitate HDO along with the higher amounts of oxygen-containing intermediates in the reaction products can be explained by the acceleration of acid-catalysed hydrolysis of methyl palmitate.

2. Results

2.1. The Effect of Preparation Conditions on the Physicochemical Properties of Ni_xP_y/γ-Al_2O_3 Catalysts

Two sets of Ni_xP_y/γ-Al_2O_3 catalysts were prepared by the incipient wetness impregnation from the phosphate- or phosphite-containing precursors (NiP_A/Al_2O_3 or NiP_I/Al_2O_3 samples, correspondingly) with the subsequent temperature-programmed reduction at 550, 600 and 650 °C. The physicochemical properties of obtained Ni_xP_y/γ-Al_2O_3 catalysts after reduction and passivation are presented in Table 1.

According to the chemical analysis (ICP-AES), the contents of Ni and P in the reduced samples of Ni_xP_y/γ-Al_2O_3 catalysts were not changed remarkably in comparison with that in precursors (Table 1). The Ni/P molar ratio is varied insignificantly in the range from 0.51 to 0.55 in the reduced NiP_A/Al_2O_3 samples (initial Ni/P ratio 0.5) and it is retained at the level of 0.34–0.35 in the reduced NiP_I/Al_2O_3 samples (initial Ni/P ratio 0.3). The Ni/P molar ratios in reduced catalysts were slightly higher than the initial Ni/P molar ratios in oxide precursors and impregnating solutions. The increase of the Ni/P molar ratio in the catalysts after reduction is caused by the formation and elimination of volatile phosphorus-containing species (namely PH_3 or P, P_2 etc.) during high-temperature reduction. The retained P could enter into the composition of nickel phosphide particles, unreduced PO_x groups [43,45], elemental phosphorus residuals [46] and $AlPO_4$ [43].

With the increase of the reduction temperature from 550 to 650 °C, the specific surface area (A_{BET}) of NiP_A/Al_2O_3 catalysts is expanded from 127 to 158 m^2/g along with the decrease of the average pore diameter (D_{pore}) from 12.7 to 10.6 nm. The specific surface area of reduced NiP_I/Al_2O_3 catalysts is decreased approximately 2-fold in comparison with γ-Al_2O_3 (101–120 m^2/g vs. 205 m^2/g of γ-Al_2O_3). The average pore diameter of reduced NiP_I/Al_2O_3 catalysts is also decreased from 13.4 nm to 8.3–9.2 nm in comparison with the γ-Al_2O_3 support. Figure S1 shows the curves of incremental pore volume distribution depending on the average pore diameter for NiP_A/Al_2O_3 and NiP_I/Al_2O_3 samples. It indicates that the mesoporous structure of the support was conserved after active component loading and reduction but the total pore volume was decreased. The textural characteristics of the catalyst could have changed because of the thermal treatment [40]. Also, the decrease of A_{BET}, D_{pore} and V_{pore} for the catalysts in comparison with alumina support is caused with the partial pore clogging by Ni_xP_y particles and phosphorus-containing compounds (PO_x groups, elemental phosphorus) or probably with the support structure rearrangement because of $AlPO_4$ formation as will be illustrated later by NMR data.

Table 1. Physicochemical properties of NiP_A/Al_2O_3, NiP_I/Al_2O_3 and NiP_I/SiO_2 catalysts.

Sample	$T_{reduction}$, °C	Elemental Content after TPR, wt%		Molar Ni/P	A_{BET}, m^2/g	D_{pore}, nm	XRD Phase	D_{XRD}, nm
		Ni	P					
NiP_A/Al_2O_3(550)	550	7.3	7.6	0.51	127	12.7	Ni Ni_3P	5.5 -
NiP_A/Al_2O_3(600)	600	7.3	7.6	0.51	130	11.9	Ni Ni_3P $Ni_{12}P_5$	5.0 4.5 12.0
NiP_A/Al_2O_3(650)	650	7.5	7.2	0.55	158	10.6	Ni_3P $Ni_{12}P_5$	7.6 11.5
NiP_I/Al_2O_3(550)	550	7.4	11.6	0.34	115	8.6	Ni_2P	3.8
NiP_I/Al_2O_3(600)	600	7.4	11.3	0.35	120	8.3	Ni_2P	3.8
NiP_I/Al_2O_3(650)	650	7.6	11.5	0.35	101	9.2	Ni_2P	4.4
NiP_I/SiO_2(600)	600	7.5	7.4	0.53	180	12.7	Ni_2P	5.5

H_2-TPR profiles of $NiPO_x$_A/Al_2O_3 precursor and $NiPO_x$_I/Al_2O_3 precursor as well as the reference $NiPO_x$_I/SiO_2 precursor are shown in Figure 1. H_2-TPR profiles of the $NiPO_x$_A/Al_2O_3

and $NiPO_x$_I/Al_2O_3 precursors are entirely different. It was indicated that the reduction of $NiPO_x$_A/Al_2O_3 precursor starts at the temperature of 525 °C. It was observed two maximums of hydrogen consumption at 725 °C and 840 °C and the hydrogen uptake does not run out up to 900 °C. According to the literature data [22,37,44], similar H_2-TPR profiles are characteristic for the reduction of nickel phosphate precursors deposited on alumina and also for the reduction of phosphate species (PO_4^{3-}, $P_2O_7^{4-}$ and $(PO_3^-)_n$) at a temperature above 720 °C [47,48]. There are no low-temperature peaks corresponding to the reduction of nickel oxide particles [49]. According to the literature data [50], the reduction of commercial aluminium phosphate and alumina-supported phosphates begins at a temperature above 700 and 800 °C, correspondingly. From the H_2-TPR profile of $NiPO_x$_I/Al_2O_3 precursor it is seen that the reduction of oxide precursors starts at the temperature of 300 °C with the formation of additional amount of hydrogen, as a result of phosphorous acid and nickel phosphites decomposition [26,51,52]. The H_2-TPR profile contains signals in the temperature range of 400–600 °C directed downward. In this temperature region phosphorous acid and phosphite-containing compounds are disproportionate to the formation of phosphine and H_3PO_4 or phosphates. In agreement with the literature data phosphine could interact with Ni^{2+} species producing nickel phosphides already at the temperature as low as 250 °C [53]. In addition, PH_3 can decompose at higher temperatures into elemental phosphorus and hydrogen. From the temperature of ~600 °C for the $NiPO_x$_I/Al_2O_3 precursor, hydrogen absorption is associated with the reduction of phosphate-containing components formed during the decomposition of phosphorous acid. Thus, it can be expected that the formation of nickel phosphide phase in the case of the phosphite-containing precursor occurs at lower reduction temperature. The H_2-TPR curve of the reference $NiPO_x$_I/SiO_2 precursor shows a similar dependence of the hydrogen uptake from temperature, however, the amount of absorbed hydrogen in the temperature range of 600–900 °C is higher for the silica-supported sample in contrast to the alumina-supported one. This fact was also confirmed by chemical analysis data showing the Ni/P molar ratio equal to 0.53 in NiP_I/SiO_2(600) sample in comparison to 0.35 in NiP_I/Al_2O_3(600) (Table 1). Such a difference between the behaviours of SiO_2- and Al_2O_3-supported catalysts is due to a stronger interaction of phosphate groups with the surface of aluminium oxide [44,54–56]. As a result, phosphate groups supported on silica are readily reduced and removed in the form of phosphine (or volatile phosphorus species), while the interaction of phosphate groups with the surface of alumina leads to the formation of alumina phosphate and surface-bonded mono-and poly-phosphates that are stable to at least 650 °C.

Based on the H_2-TPR data of the oxide precursors and the literature data [42], the reduction temperatures of 550–650 °C were chosen to investigate the nickel phosphide phase formation on alumina. The XRD patterns of the γ-Al_2O_3 support, as well as alumina-supported nickel phosphide catalysts differing in the precursor natures and the reduction temperatures, are shown in Figures 2 and 3.

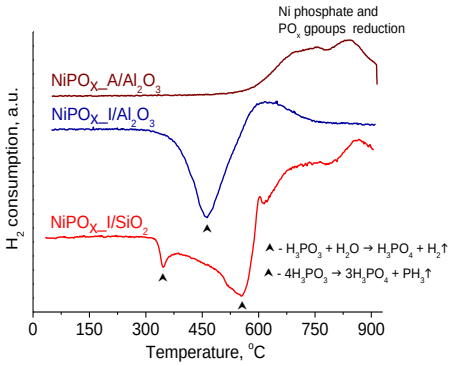

Figure 1. H_2-TPR profiles of $NiPO_x$_A/Al_2O_3, $NiPO_x$_I/Al_2O_3 and $NiPO_x$_I/SiO_2 precursors.

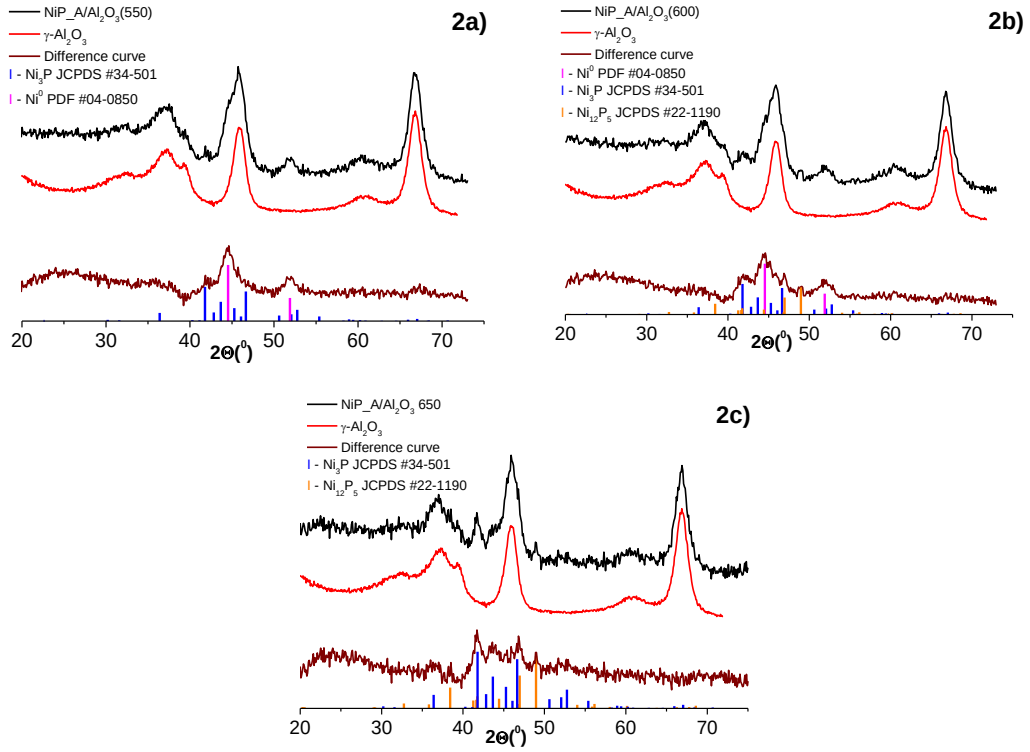

Figure 2. XRD patterns of NiP_A/Al_2O_3 catalyst prepared from phosphate precursor and reduced at temperature of 550 °C (**a**), 600 °C (**b**) or 650 °C (**c**), γ-Al_2O_3 support and the difference curve.

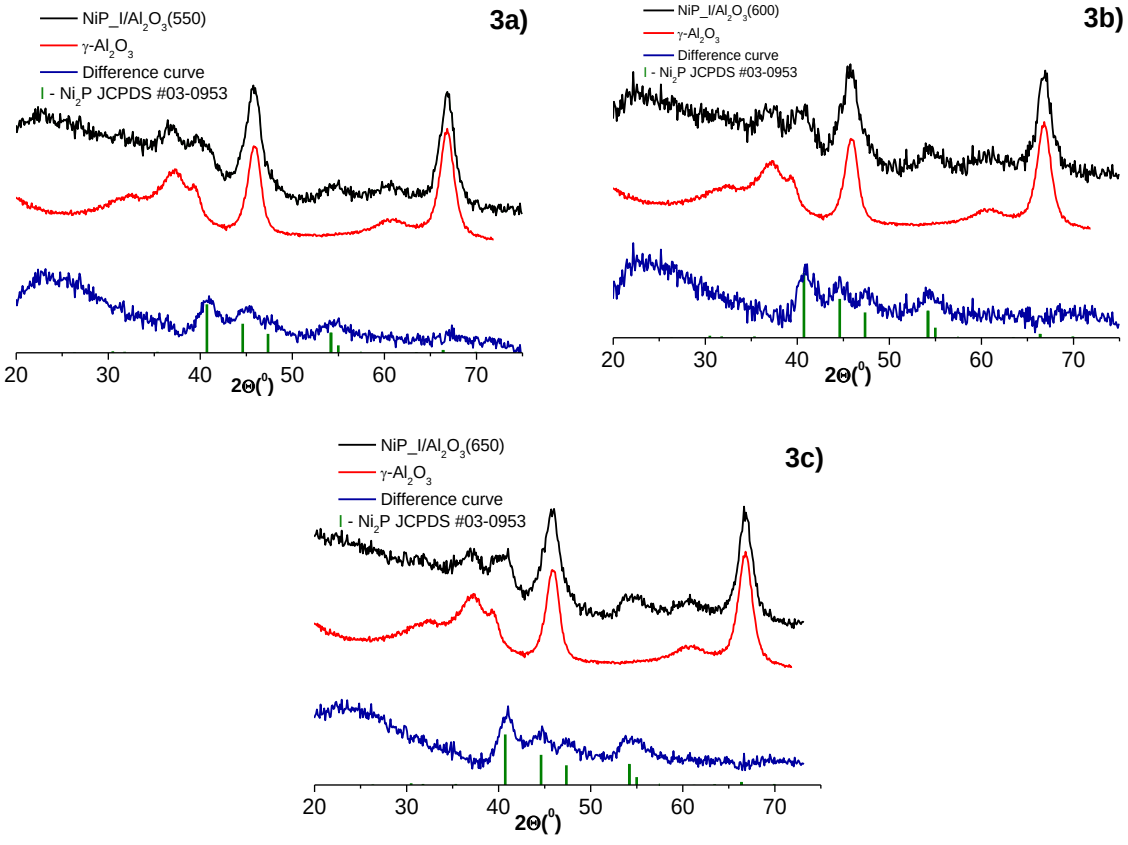

Figure 3. XRD patterns of NiP_I/Al_2O_3 catalyst prepared from phosphite precursor and reduced at temperature of 550 °C (**a**), 600 °C (**b**) or 650 °C (**c**), γ-Al_2O_3 support and the difference curve.

The XRD patterns of NiP_A/Al_2O_3 and NiP_I/Al_2O_3 samples reduced at 550–650°C contain characteristic diffraction peaks from γ-Al_2O_3 (PDF No. 29-0063) and nickel-containing phases. The difference intensity curves obtained by the subtraction of the XRD curve of the alumina from the catalyst ones help us to identify the Ni-containing phases.

For NiP_A/Al_2O_3(550) sample the predominant phase was metallic Ni^0 (PDF No. 04-0850) with average crystallite size equalled to 5.5 nm (Figure 2a, Table 1). Weak intensity peaks characteristic of Ni_3P phase (JCPDS No. 34-501) were also observed. With the reduction temperature increase to 600 °C the predominant phase in NiP_A/Al_2O_3(600) sample has remained the metallic Ni^0 (D_{XRD} = 5.0 nm). Also, the presence of Ni_3P and $Ni_{12}P_5$ (JCPDS No. 22-1190) phases was indicated (Figure 2b). The estimated Ni_3P and $Ni_{12}P_5$ crystallite sizes were 4.0–4.5 nm and 12 nm, respectively. The further reduction of temperature increase to 650 °C led to the disappearance of metallic nickel and the predominant Ni_3P phase (D_{XRD} = 7.6 nm) formation with an additional amount of $Ni_{12}P_5$ phase (D_{XRD} = 11.5 nm) (Figure 2c). Thus, it was shown that for the set of NiP_A/Al_2O_3 catalysts obtained from phosphate precursor increase in the reduction temperature from 550 to 650 °C promotes the formation of the Ni_3P and $Ni_{12}P_5$ phases and the average crystallite sizes growth. Nevertheless, the desired Ni_2P phase has not been obtained.

The XRD patterns of NiP_I/Al_2O_3 catalysts obtained from phosphite precursor are shown in Figure 3. Only the characteristic diffraction peaks corresponding to Ni_2P phase (JCPDS No. 03-0953) are found in the difference curve. With the growth of the reduction temperature from 550 to 650 °C the estimated Ni_2P crystallites sizes are increased slightly from 3.8 nm to 4.4 nm. So, it is shown that using the phosphite-containing precursor makes it possible to produce highly dispersed Ni_2P crystallites on γ-Al_2O_3 after reduction at 550–650 °C. According to XRD analysis, the NiP_I/SiO_2(600) catalyst also contains the characteristic peaks of the Ni_2P phase with D_{XRD} = 5.5 nm (Figure S2) [26].

Figure 4 shows the TEM images of NiP_A/Al_2O_3(650) and NiP_I/Al_2O_3(600) catalysts prepared from different precursors. The nickel phosphide particles with different size ranged in the region from 4.0 to 50 nm were observed in the NiP_A/Al_2O_3(650) sample (Figure 4a). Also, individual particles with the size up to 100 nm were found. On the contrary, NiP_I/Al_2O_3(550–650) samples demonstrate a uniform distribution of the nickel phosphide particles on the alumina surface (Figure 4b). The mean Ni_2P particle diameters of the NiP_I/Al_2O_3(550), NiP_I/Al_2O_3(600) and NiP_I/Al_2O_3(650) samples were estimated, equalling 5.1 nm, 5.6 nm and 6.0 nm, correspondingly. Thus, the mean Ni_2P particle diameters of NiP_I/Al_2O_3 catalysts slowly increased with the reduction temperature growth from 550 to 650 °C. The TEM image of NiP_A/Al_2O_3(650) catalyst (Figure S3a) reveals crystal lattice fringes with the d-spacing value of 2.16 Å, 2.47 Å and 2.83 Å corresponding to the (231), (031) and (130) reflections of the Ni_3P phase (PDF No. 34-501), respectively. Also, it was found the crystal lattice fringes with the d-spacing value of 2.12 Å and 2.55 Å corresponding to the (121) and (202) reflections of $Ni_3(PO_4)_2$ (PDF No. 70-1796) that proved the formation of a thin layer of nickel phosphate after passivation covered the nickel phosphide particles (Figure S3a). The TEM images of NiP_I/Al_2O_3(600) catalyst in Figure S3b exhibit crystal lattice fringes with the d-spacing value of 2.03 Å and 2.22 Å corresponding to the (021) and (111) reflections of the Ni_2P crystalline phase (PDF No. 63-3444).

The nature of the precursor of the active component affects not only the morphological features of the formed nickel phosphide particles on the alumina surface but also the number of acid sites on the surface. The NH_3-TPD technique was employed to explore the acidic properties of samples. Before NH_3-TPD experiments, the nickel phosphide catalyst precursors were reduced in situ in Autosorb-1 apparatus. Figure 5a,b shows the NH_3-TPD curves of NiP_A/Al_2O_3 and NiP_I/Al_2O_3 catalysts, as well as the γ-Al_2O_3 support. The quantities of acid sites estimated by integration and further deconvolution of NH_3 desorption peaks of applied materials are listed in Table 2.

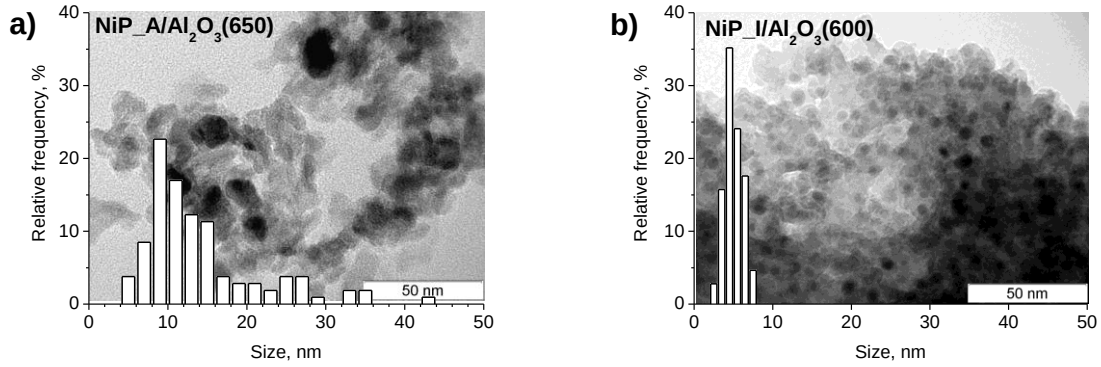

Figure 4. TEM images of Ni_xP_y/γ-Al_2O_3 catalysts prepared from different precursors: (**a**) NiP_A/Al_2O_3(650) and (**b**) NiP_I/Al_2O_3(600).

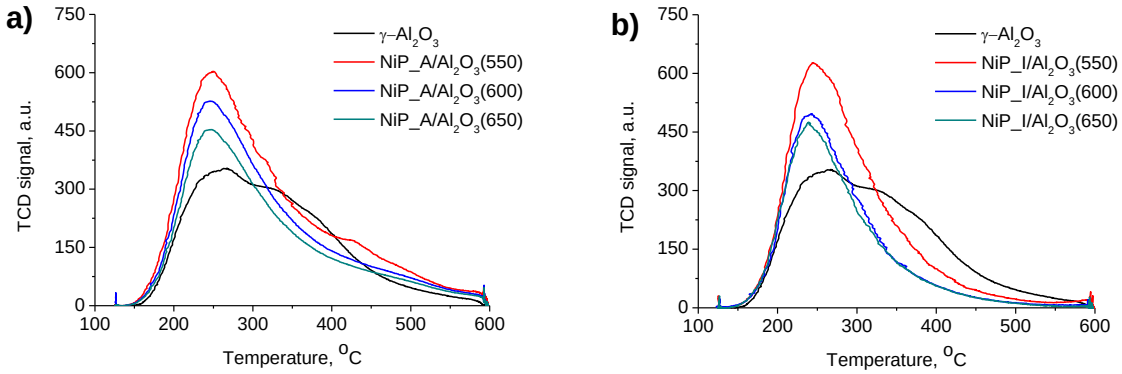

Figure 5. NH_3-TPD profiles of Ni_xP_y/Al_2O_3 catalysts prepared from different precursors: (**a**) NiP_A/Al_2O_3 and (**b**) NiP_I/Al_2O_3 and γ-Al_2O_3 sample.

Table 2. Summary data of NH_3-TPD and MAS NMR methods for NiP_A/Al_2O_3 and NiP_I/Al_2O_3 catalysts, γ-Al_2O_3 support as well as SiO_2 and NiP_I/SiO_2 catalyst.

Sample	$T_{reduction}$, °C	NH_3-TPD			MAS NMR	
		T_{max}, °C	Quantity, µmol/g	Overall Quantity, µmol/g	Ni_xP_y, at.% ^{31}P NMR	$AlPO_4$, at.% ^{27}Al NMR
γ-Al_2O_3	-	237 335	106 315	421	-	-
NiP_A/Al_2O_3(550)	550	249 311	298 326	624		
NiP_A/Al_2O_3(600)	600	245 334	287 222	510		
NiP_A/Al_2O_3(650)	650	245 306	246 194	440	35 ± 10	25 ± 2
NiP_I/Al_2O_3(550)	550	244 308	322 155	477	39 ± 10	22 ± 2
NiP_I/Al_2O_3(600)	600	244 285	223 130	354	39 ± 10	25 ± 2
NiP_I/Al_2O_3(650)	650	238 278	193 133	326	60 ± 10	30 ± 2
SiO_2	-	231	84	84	-	-
NiP_I/SiO_2(600)	600	241 299	116 47	163	92	-

NH_3-TPD curve of γ-Al_2O_3 has two desorption peaks of ammonia centred at 237 °C and 335 °C. The first desorption peak around 237 °C is usually attributed to the sites with the weakest acidity on the boundary of physiosorbed and chemisorbed ammonia, the second desorption peak at the temperature of 337 °C was assigned to the moderate strength acid sites [57]. The total acidity of γ-Al_2O_3 support is equal to 421 μmol/g. On the NH_3-TPD curves of NiP_A/Al_2O_3 and NiP_I/Al_2O_3 catalysts reduced at 550, 600 and 650 °C, two desorption peaks of ammonia centred at the temperatures of 238–249 °C and 278–334 °C were also observed. According to the literature data, the acid sites of nickel phosphides are ascribed to weak Brønsted and Lewis acid sites specified by the presence of unreduced P-OH species and nickel sites with small positive charge ($Ni^{\delta+}$) due to the electron transfer from the metal to the P atoms, respectively [44,58,59].

With the increase of the reduction temperature from 550 to 650 °C the overall acidity of catalysts is decreased from 624 to 440 μmol/g and from 477 to 326 μmol/g for the samples obtained from the phosphate and phosphite precursor, correspondingly. The number of the weakest acid sites with T_{max} = 238–249 °C in all catalysts is increased in comparing with the alumina support. Whereas the amount of the moderate strength acid sites with T_{max} = 278–334 °C is retained only in NiP_A/Al_2O_3 550 sample and decreased in the other investigated catalysts. The decrease of the amount of the moderate strength acid sites is caused by the shielding of the part of the alumina surface by the surplus of phosphorus-containing species especially in the samples prepared from the phosphite precursor. Earlier it was reported that the alumina-supported catalysts prepared from phosphate precursors also contain the increased number of Brønsted acid sites referring to O=P(OH)$_2$-O-Al species formed after interaction of phosphate precursor and alumina surface OH-groups or to free O=P(OH)$_3$ entities interacting with the alumina surface via H-bonding [54,56].

The total acidity of silica-supported NiP_I/SiO_2(600) catalyst is lower than the acidity of alumina-supported samples (Table 2). On the NH_3-TPD curve of NiP_I/SiO_2(600) catalyst, the main desorption peak of ammonia centred at the temperature of 241 °C corresponding to weak acidic sites and the minor peak corresponding to moderate strength acid sites at 299 °C were observed.

Figure 6 displays the ^{31}P 14 kHz MAS NMR spectrum of NiP_A/Al_2O_3 catalyst after reduction at 650 °C, which can be divided into two main regions. The narrow region around 0 ppm corresponds to compounds comprising different PO_x groups, including phosphorus oxides, phosphates, phosphites and surface PO_x groups [26,46,60–62]. The broad part of the spectrum stretching from ~500 to ~5000 ppm contains resonances of different metallic-like compounds of phosphorus, namely, nickel phosphides [26,46,63]. The most prominent signal in this part of the spectrum is located at ~1800 ppm. According to literature data, such shift corresponds to Ni_3P phase [46]. This line lies upon a wide resonance covering the area from ~1000 to ~2500 ppm, which can contain signals from several other nickel phosphides. The downfield shoulder of this resonance indicates the presence of $Ni_{12}P_5$ phase that gives rise to two signals at ~2250 and ~1950 ppm. The upfield shoulder may correspond to NiP, Ni_5P_4 and Ni_2P phases, however, the latter has two inequivalent sites with chemical shifts of ~1500 and ~4000 ppm and there is no signal with 4000 ppm shift on the spectrum, so it is unlikely that the sample contains Ni_2P particles.

Since the line of Ni_3P is relatively narrow, we can assume that the particles of this phase are regular to some extent; moreover, this assumption is confirmed by the fact that this phase was observed earlier in the XRD pattern. On the contrary, the lines corresponding to other phases are too broad and shapeless, which can mean that their particles are small or inhomogeneous. Nonetheless, we can estimate the relative amount of phosphorus in nickel phosphides (roughly 35%, Table 2) in this sample from the ratio of spectral intensities integrated over the "phosphide" region (500–4500 ppm) and over the entire spectrum. The remaining phosphorus is present in the sample as different PO_x groups including $AlPO_4$.

Figure 7 shows the experimental 14 kHz MAS ^{27}Al NMR spectrum of NiP_A/Al_2O_3(650) catalyst and its decomposition into three separate lines. Two of them belong to γ-Al_2O_3 (octahedral site of Al_2O_3 (O) at ~10 ppm and tetrahedral site of Al_2O_3 (T) at ~70 ppm) and the third corresponds to the

AlO_4 tetrahedra of $AlPO_4$ [54,64]. All of the lines possess an irregular shape well described by the Simple Czjzek Model of Gaussian distribution of quadrupolar parameters [65]. Using this model, we deconvoluted the spectrum into the signals from γ-Al_2O_3 and $AlPO_4$ and determined the relative amount of the latter equal to ~25 at% (Table 2).

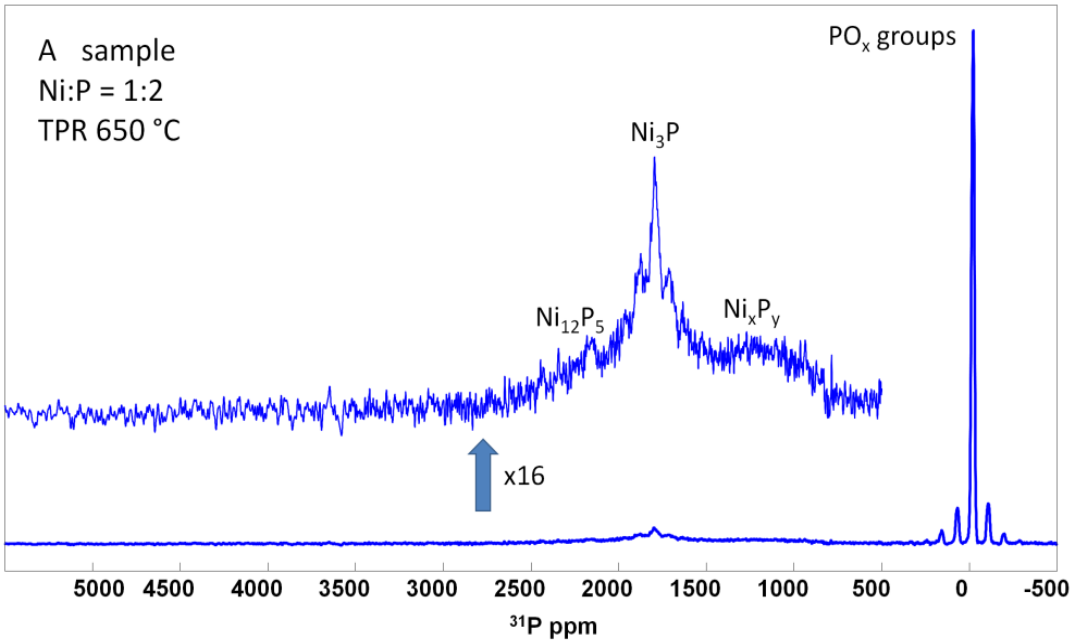

Figure 6. 14 kHz MAS ^{31}P NMR spectrum of NiP_A/Al_2O_3(650) catalyst. The inset shows the "phosphide" region multiplied by 16 for clarity.

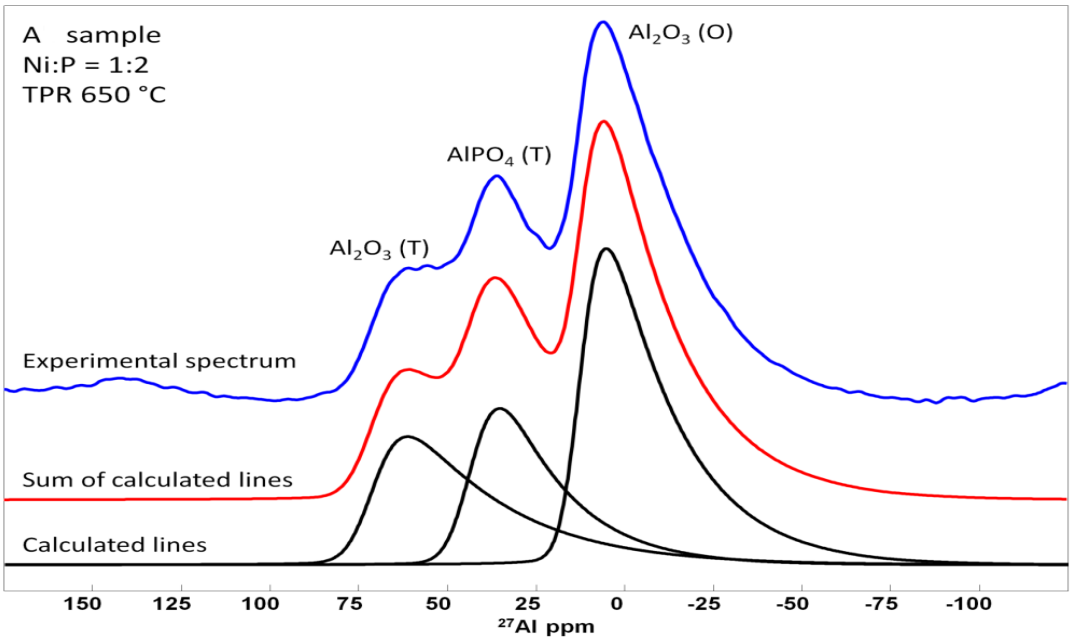

Figure 7. Blue–experimental 14 kHz MAS ^{27}Al NMR spectrum of NiP_A/Al_2O_3(650) sample, black–theoretic calculated lines corresponding to different Al_2O_3 and $AlPO_4$ sites, red–sum of the calculated lines.

Figure 8 displays the "phosphide" regions of 14 kHz MAS ^{31}P NMR spectra of NiP_I/Al_2O_3(550–650) catalysts reduced from phosphite precursor at the temperatures of 550, 600 and 650 °C. These spectra contain two very broad resonances centred at ~1500 and ~4000 ppm characteristic of Ni_2P phase, though, very disordered. Another signal with very large FWHM is located around 2500 ppm and probably connected with $Ni_{12}P_5$ phase. Quantitative analysis of spectra of samples with different reduction temperatures gives the following result: relative content of phosphorus included in phosphides in the sample reduced at 650 °C is much higher (~60 at% vs. ~40 at%) than in the samples reduced at lower temperatures (Table 2), while the absolute intensity of lines in the "phosphide" region of these samples is close (Figure S4). It means that some PO_x groups are reduced only at temperatures higher than 600 °C probably resulting in the formation of phosphine or some other volatile phosphorus compound, while no additional nickel phosphides are formed.

14 kHz MAS ^{27}Al NMR spectra of NiP_I/Al_2O_3 samples reduced at 550, 600 and 650 °C display the same three lines belonging to γ-Al_2O_3 (~10 and ~70 ppm) and $AlPO_4$ (~40 ppm) as the spectrum of NiP_A/Al_2O_3 sample (Figure 9). From deconvolution of these spectra into separate lines, we calculated the relative content of Al in the form of $AlPO_4$ that was equal to 22–30 at% for all samples (Table 2), while the support maintained the near to perfect ratio Al_2O_3 (O)/Al_2O_3 (T) = 1/2. From the results of ^{27}Al and ^{31}P NMR, it is likely that while the amount of $AlPO_4$ slightly grows with increasing reduction temperature, the overall phosphorus load of samples decreases due to the reduction of excess supported PO_x groups with the formation of phosphine or some other volatile phosphorus compound.

Thus, ^{31}P and ^{27}Al MAS NMR of NiP_A/Al_2O_3(650) sample confirm the formation of aluminium phosphates in catalysts obtained by TPR of phosphate precursor, which hinders the formation of the desired Ni_2P phase and leads to an irreversible change in composition and textural characteristics of γ-Al_2O_3 support according to literature data [37,40]. Neither the nature of the precursor nor the temperature of reduction can help to prevent the formation of aluminium phosphate on the surface of the catalyst. Summarizing the XRD, TEM and NMR results of catalyst characterization it could be concluded that Ni_3P and $Ni_{12}P_5$ particles supported on the surface of γ-Al_2O_3 are formed after reduction of phosphate precursor at the temperature of 650 °C, while Ni_2P particles are produced from phosphite precursor after reduction in the temperature range of 550–650 °C.

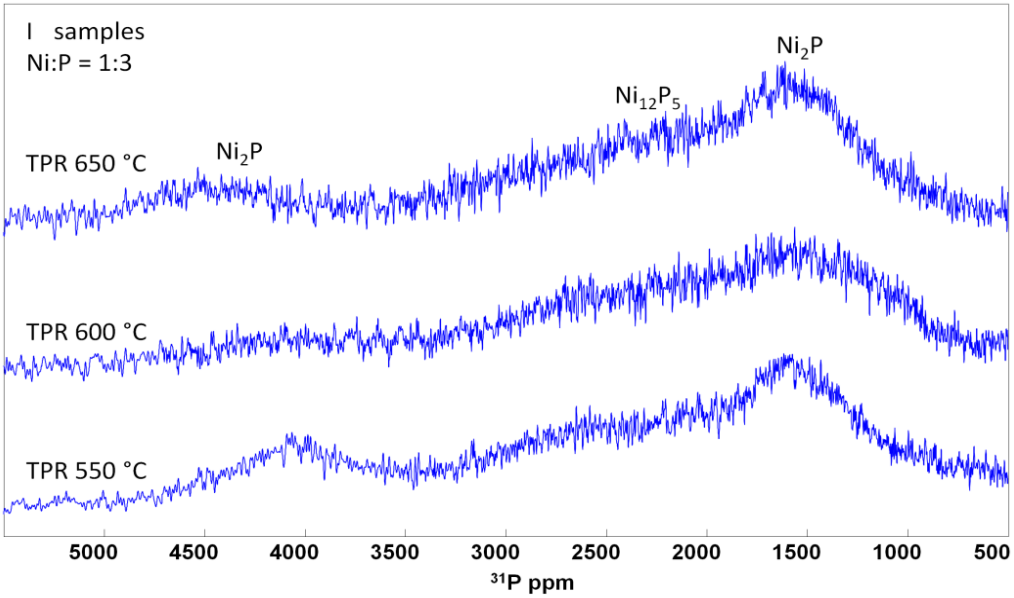

Figure 8. 14 kHz MAS ^{31}P NMR spectra of NiP_I/Al_2O_3 samples reduced at 550, 600 and 650 °C. The region with PO_x groups is not shown.

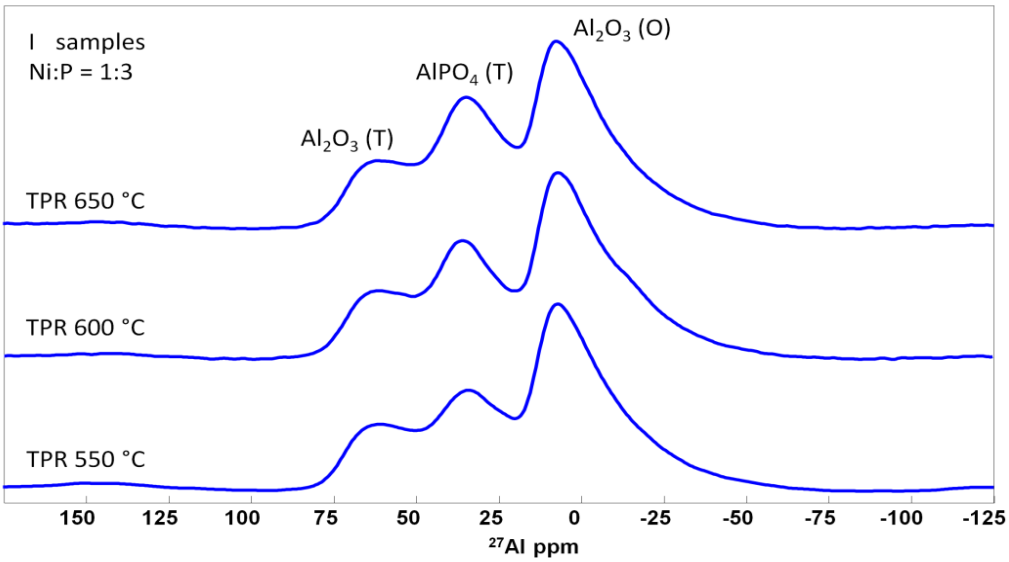

Figure 9. 14 kHz MAS ^{27}Al NMR spectra of NiP_I/Al_2O_3 samples reduced at 550, 600 and 650 °C.

2.2. Catalytic Properties of Ni_xP_y/γ-Al_2O_3 Catalysts in Methyl Palmitate HDO

2.2.1. The Effect of Preparation Conditions on the Catalytic Properties of Ni_xP_y/γ-Al_2O_3 Catalysts in Methyl Palmitate HDO

To evaluate the impact of the preparation conditions on the catalytic properties of the Ni_xP_y/Al_2O_3 systems in the HDO of methyl palmitate several alumina-supported nickel phosphide catalysts differing in the precursor nature and reduction temperature were studied. It was shown in the previous section that the reduction of the samples prepared from phosphite precursor at 550, 600 and 650 °C gives rise to Ni_2P phase supported on alumina (NiP_I/Al_2O_3 catalysts). The Ni_3P phase with the admixture of $Ni_{12}P_5$ and some unreduced species have been observed in NiP_A/Al_2O_3 catalyst prepared from phosphate precursor, even after reduction at 650 °C. Therefore, NiP_A/Al_2O_3 catalyst (reduced at 650 °C) and series of NiP_I/Al_2O_3 samples, prepared by reduction at 550, 600 and 650 °C, were chosen for the comparative study in the HDO of methyl palmitate. The reaction was carried out at the temperature of 290 °C, hydrogen pressure — 3.0 MPa, H/C ratio — 600 Nm^3/m^3, methyl palmitate LHSV — 2.4-12 h^{-1} for 8 h, during this time the concentrations of the reagent and the products have reached a constant value.

The catalytic properties of Ni_xP_y/Al_2O_3 catalysts are shown in Figure 10. The presented data indicate that NiP_A/Al_2O_3 catalyst is significantly inferior in activity compared to the NiP_I/Al_2O_3 samples and this tendency is conserved within the temperature region of 250–330 °C (Figure S5). The higher activity of NiP_I/Al_2O_3 catalysts points out that $Ni_3P/Ni_{12}P_5$ phases display lower activity in the HDO of methyl palmitate then the Ni_2P one. These results agree with the data obtained earlier for silica-supported systems, demonstrating the higher activity of Ni_2P/SiO_2 catalyst in comparison with the $Ni_{12}P_5/SiO_2$ system [17,20,27]. NiP_I/Al_2O_3 catalysts also revealed higher selectivity to C_{18} in comparison with NiP_A/Al_2O_3, the same tendency was observed in the HDO of methyl laurate [17], methyl oleate [20] and methyl palmitate [27] over Ni_2P/SiO_2 and $Ni_{12}P_5/SiO_2$ catalysts. According to the proposed explanation, the enhancing of the positive charge of metal Ni sites upon transition from Ni_3P and $Ni_{12}P_5$ to Ni_2P favours the activation of C=O groups and promotes the direct HDO reactions [17]. The activity of NiP_I/Al_2O_3 catalysts goes through the maximum with the increase of reduction temperature from 550 to 650 °C the optimal temperature being 600 °C (Figure 10). Consequently, this sample, designated further as NiP_I/Al_2O_3 was chosen for detailed study in the HDO of methyl palmitate.

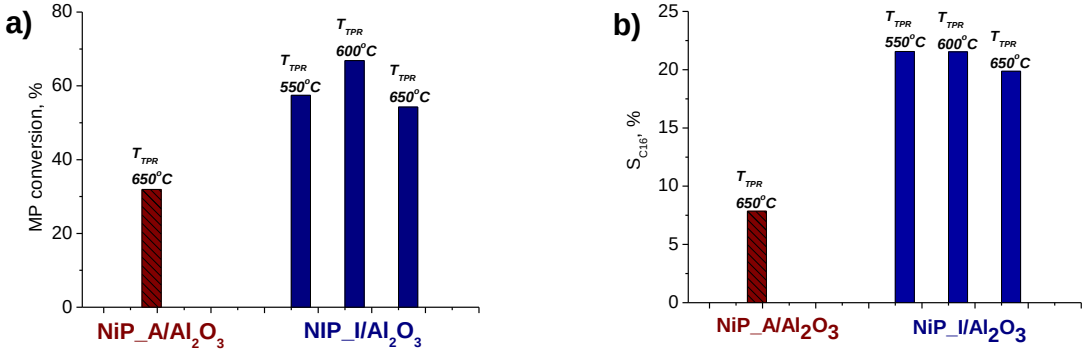

Figure 10. Conversion (**a**) and selectivity (**b**) of NiP_A/Al_2O_3 and NiP_I/Al_2O_3 catalysts in HDO of methyl palmitate (P_{H2} = 3.0 MPa, T = 290 °C, H_2/feed = 600 Nm^3/m^3, methyl palmitate LHSV = 9 h^{-1}).

2.2.2. Comparison of Ni_2P/Al_2O_3 and Ni_2P/SiO_2 Catalysts in the HDO of Methyl Palmitate

Figure 11 shows the dependencies of the conversion of methyl palmitate and oxygen-containing compounds on the reaction temperature over NiP_I/Al_2O_3 (Ni_2P/Al_2O_3) and NiP_I/SiO_2 (Ni_2P/SiO_2) catalysts. NiP_I/SiO_2 catalyst was prepared using the same procedure and contained the comparable amount of Ni and the mean particle diameter equalled to 5.5 nm (Table 1). In all experiments, the conversions of methyl palmitate and O-containing compounds are increased with the growth of temperature; wherein the NiP_I/SiO_2 catalyst displays lower values of conversion. The minor difference between the dependencies of methyl palmitate and O-containing compounds conversions on temperature was observed over NiP_I/SiO_2 catalyst, indicating that only small amounts of oxygen-containing intermediates are present in the reaction mixture. Indeed, the results of liquid product analysis showed only negligible amounts of oxygen-containing intermediates among the reaction products in the whole temperature range and the main products are hexadecane and pentadecane (Figure 12). Such behaviour is typical for all silica-supported Ni_xP_y systems, regardless of the precursor, Ni content or preparation conditions [24–27], pointing out that in the presence of Ni_xP_y/SiO_2 catalysts the rate of methyl palmitate conversion is lower than the rates of oxygenated intermediates conversion. As a consequence, the rate of methyl palmitate transformation determines the overall rate of methyl palmitate HDO over NiP_I/SiO_2 catalyst. The conclusion was confirmed in the additional experiments by the comparison of HDO conversion rate of the methyl laurate and the corresponding intermediate compounds: lauric acid, dodecanal and dodecanol (Figure S6). It was shown, that in the presence of NiP_I/SiO_2 catalyst methyl laurate demonstrated the lowest conversion among the listed oxygen-containing substrates.

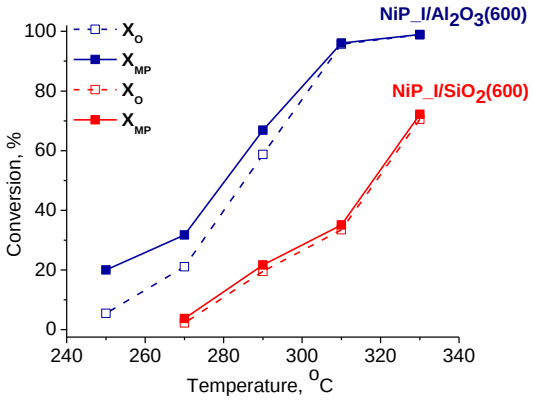

Figure 11. Temperature effect on the conversion of methyl palmitate (solid symbols, solid lines) and oxygen-containing compounds (empty symbol, dash lines) over NiP_I/Al_2O_3 and NiP_I/SiO_2 catalysts (P_{H2} = 3.0 MPa, T = 250–330°C, H_2/feed = 600 Nm^3/m^3, methyl palmitate LHSV = 3.6–9 h^{-1}).

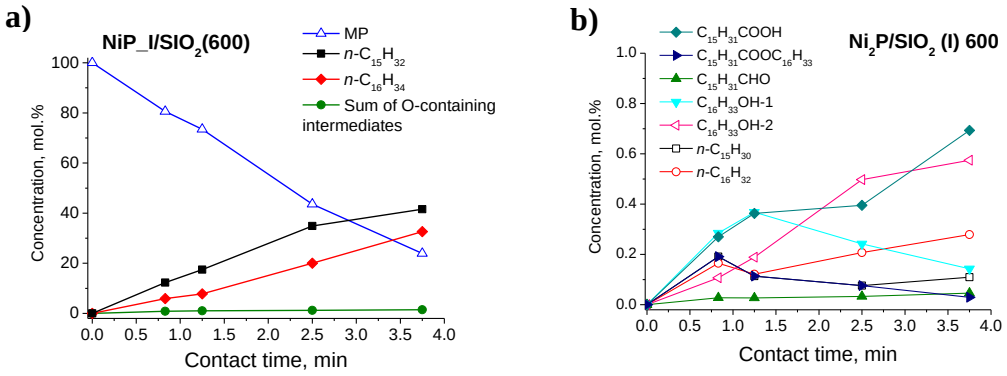

Figure 12. Concentration profiles of the liquid-phase components during methyl palmitate HDO over NiP_I/SiO_2(600) catalyst: (**a**) MP, C_{15} and C_{16} hydrocarbons and sum of oxygen-containing intermediates; (**b**) the observed intermediates (P_{H2} = 3.0 MPa, T = 290 °C, H_2/feed = 600 Nm^3/m^3, contact time = 0.83–3.75 min).

The comparison of NiP_I/Al_2O_3 and NiP_I/SiO_2 catalysts in methyl palmitate HDO shows that the use of γ-Al_2O_3 as the support allows the significant increase of the methyl palmitate conversion. So, the conversion of methyl palmitate was raised from 22 to 67% at 290 °C and from 35 to 96% at 310 °C when NiP_I/Al_2O_3 catalyst was used instead of NiP_I/SiO_2 (Figure 11). It should be noted, that both catalysts demonstrated stable time-on-stream activity, at least for 20 hours (Figure S7). As opposed to NiP_I/SiO_2 catalyst, a significant difference was observed between the conversion of methyl palmitate and the conversion of oxygen-containing compounds in the HDO of methyl palmitate over NiP_I/Al_2O_3 catalyst at 250–290 °C. Besides, the appreciable amounts of oxygen-containing intermediates, like palmitic acid, hexadecanal, hexadecanols and palmityl palmitate were determined among the reaction products (Figure 13). The difference in the content of oxygenated compounds among the products of methyl palmitate HDO over NiP_I/SiO_2 and NiP_I/Al_2O_3 catalysts is seen explicitly in Figure 14 demonstrating the content of oxygenated intermediates at the same conversion of methyl palmitate (about 57%). The observed results indicate that the rate of methyl palmitate conversion over alumina-supported catalysts is higher than the conversion rates of intermediate oxygenating compounds. To explain the observed difference in the behaviour of silica-supported and alumina-supported Ni_2P catalysts the possible routes of methyl palmitate transformation should be analysed.

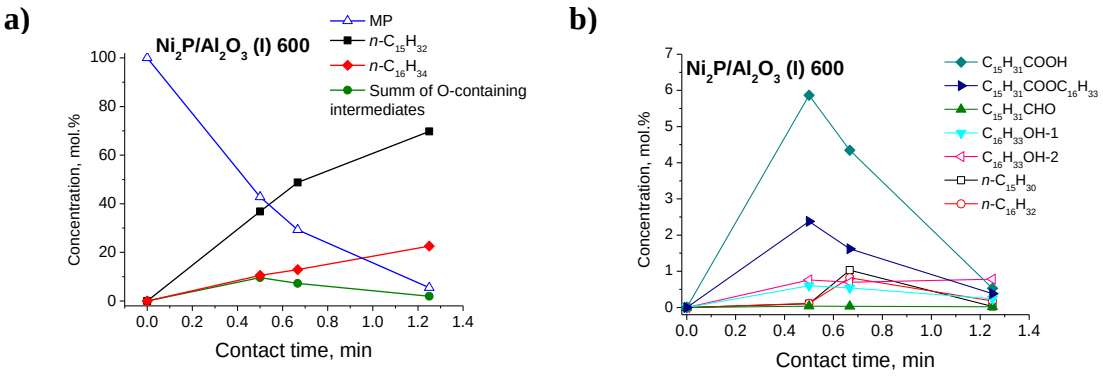

Figure 13. Concentration profiles of the liquid-phase components during methyl palmitate HDO over NiP_I/Al_2O_3(600) catalyst: (**a**) MP, C_{15} and C_{16} hydrocarbons and sum of oxygen-containing intermediates; (**b**) the observed intermediates (P_{H2} = 3.0 MPa, T = 290 °C, H_2/feed = 600 Nm^3/m^3, contact time = 0.50–1.25 min).

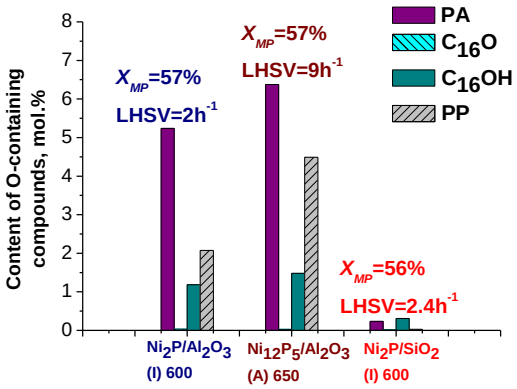

Figure 14. Composition of oxygen-containing compounds depending on the catalyst: NiP_I/Al_2O_3(600), NiP_A/Al_2O_3(650) and NiP_I/SiO_2(600) catalysts at T = 290 °C, P_{H2} = 3.0 MPa, H_2/feed = 600 Nm^3/m^3 and methyl palmitate LHSV was adjusted to obtain nearly the same methyl palmitate conversion (2.4–12 h^{-1}). Notation: PA–palmitic acid, $C_{16}O$–hexadecanal, $C_{16}OH$–hexadecanol, PP–palmityl palmitate.

2.2.3. Reaction Scheme

The reaction networks of methyl palmitate transformation over silica-supported nickel phosphide catalysts were widely discussed in the literature [17,19,22–25,27]. Scheme 1 represents the reaction network for methyl palmitate HDO, including the intermediate and final product of methyl palmitate conversion. Palmitic acid and hexadecanal are usually considered as the primary products of methyl palmitate hydroconversion. Palmitic acid can be produced through the hydrogenolysis of the C-O bond in the methoxy group over metal sites or via hydrolysis over acid sites, giving methane or methanol, correspondingly [17,25,27,31]. Hydrogenolysis of the ester C-O bond over metal sites leads to hexadecanal and methanol. Further conversion of palmitic acid was proposed to give pentadecane through the decarboxylation reaction or hexadecanal as a result of hydrogenation. Decarboxylation of palmitic acid can proceed to some extent over NiP_I/SiO_2, NiP_I/Al_2O_3 and NiP_A/Al_2O_3 catalysts because the small amounts of CO_2 were observed among the gas products but the primary route of pentadecane formation is decarbonylation of hexadecanal. The sum of CO and CO_2 correlates with pentadecane content (Figure S8). In addition, hexadecanal gives hexadecanol-1 via hydrogenation that in turn is transformed to hexadecane through the subsequent reactions of dehydration to hexadecene and hydrogenation to hexadecane.

The scheme of methyl palmitate conversion includes some parallel and sequential transformations that can take place with the participation of acidic (ether hydrolysis, alcohol dehydration) and metal sites (hydrogenation and hydrogenolysis reactions). It is known that nickel phosphides are characterized by the presence of metallic and acidic centres, caused by an ensemble (geometric) and/or ligand (electronic) effect of phosphorus [66,67]. Taking in mind the inertness of SiO_2, the mechanism of ester conversion over NiP_I/SiO_2 catalyst is determined by the electronic properties of the metal sites and the acidity of the nickel phosphide phase. It was shown, that nickel phosphide has both Lewis and Brønsted acid sites, that are usually ascribed to the positively charged metal cations ($Ni^{\delta+}$) and surface P-OH groups, respectively [17,58]. The correlation was also found between the acidity of Ni_2P/SiO_2 catalysts, differing in precursor and preparation conditions and the content of phosphate groups determined by means of ^{31}P NMR [26,27]. It was proposed, that P-OH groups of silica-supported Ni_2P participate in the hydrolysis of aliphatic ester (methyl laurate) as well as assist the conversion of methyl laurate adsorbed on the metal sites via decarbonylation or hydrogenation reactions [17].

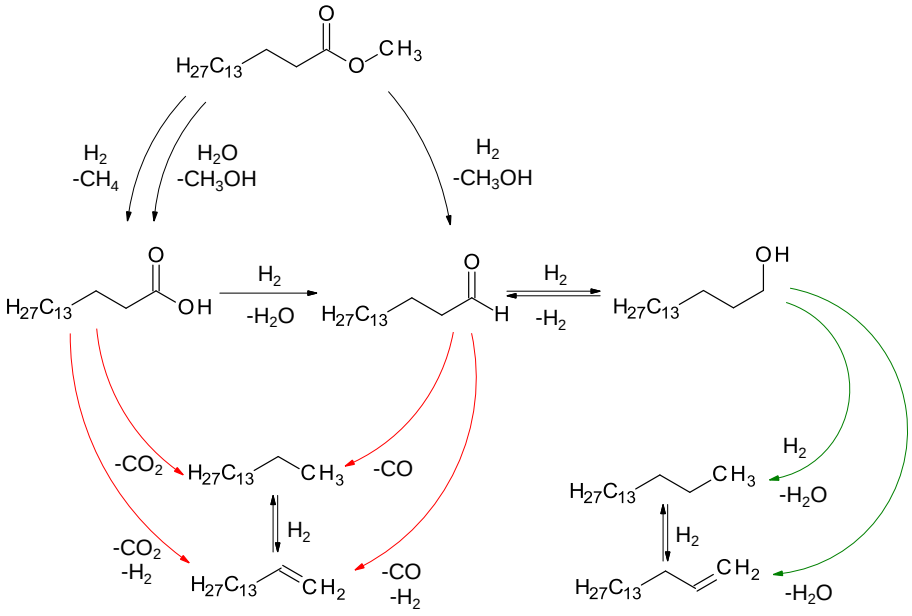

Scheme 1. Probable reaction network for HDO of methyl palmitate. Red lines–the decarboxylation and decarbonylation routes, green lines–the hydrodeoxygenation route.

The higher activity of NiP_I/Al_2O_3 catalyst in methyl palmitate HDO along with the higher production of palmitic acid in the reaction products can be explained by the participation of acid sites on the alumina support in the conversion of methyl palmitate through hydrolysis route. Indeed, the alumina-supported Ni_2P catalyst is characterized by the higher amount of acid sites in comparison with NiP_I/SiO_2 sample according to NH_3-TPD data (Table 2). It is well established, that alumina can provide the acid-catalysed reactions, such as hydrolysis, dehydration and esterification [32,35,40,68]. In our case the exact nature of acid sites on the surface of NiP_I/Al_2O_3 catalyst is undisclosed. NiP_I/Al_2O_3 catalyst produces the increasing amounts of the product of acid-catalysed esterification, namely palmityl palmitate (Figure 14), thereby indirectly confirming our assumption about the acceleration of acid-catalysed reactions over alumina-supported Ni_2P in comparison with silica-supported one. Despite on the higher acidity of NiP_A/Al_2O_3 catalyst in comparison with NiP_I/Al_2O_3 sample, NiP_A/Al_2O_3 catalyst displays lower activity in methyl palmitate hydrodeoxygenation. This observation can be explained by the assumption that lower activity of $Ni_3P/Ni_{12}P_5$ in metal-catalysed reactions led to the accumulation of oxygen-containing intermediates that retard the reversible hydrolysis reaction. Therefore, the balance between active metal sites of Ni_2P and acid sites of support is necessary for the design of the efficient catalyst for the fatty acid esters hydrodeoxygenation. The obtained results prove our assumption that the activity of the phosphide catalysts in the HDO of aliphatic esters can be improved by the employment of the support with the acidic properties instead of silica [31]. Detailed kinetic experiments may subsequently throw light on the mechanism of methyl palmitate hydrodeoxygenation and help to evaluate the contribution of metal- and acid-catalysed reactions that take place over multifunctional catalysts.

3. Materials and Methods

3.1. Materials

Commercial γ-Al_2O_3 of "VGO" brand (A_{BET} – 205 m^2/g, pore volume – 0.70 cm^3/g, average pore diameter – 13.6 nm) and SiO_2 of "KSKG" brand (A_{BET} – 300 m^2/g, pore volume – 0.80 cm^3/g, average pore diameter – 10.6 nm) were purchased from "Promkataliz" Ltd. (Ryazan, Russia) and «ChromAnalit» Ltd. (Salavat, Russia), respectively. Prior to use for catalyst preparation, granules of support were dried at 110 °C for 4 h and calcined at 500 °C for 4 h. Afterward, it was crushed and sieved to a fraction

of 0.25–0.50 mm. $Ni(NO_3)_2 \cdot 6H_2O$ ("Reakhim," Samara , Russia, ≥99%), $Ni(OH)_2$ ("Acros Organics," New Jersey, NJ, USA, ≥98%), $(NH_4)_2HPO_4$ ("Alfa Aesar," Ward Hill, MA, USA, technical grade, $P_2O_5 \leq 53$ wt%), H_3PO_3 ("Sigma-Aldrich," Saint Louis, MO, USA, ≥97%) and HNO_3 ("Reakhim," Samara, Russia, ≥70%) were used for the catalyst preparation. The chemical products utilized in the reactivity investigation were methyl palmitate ($C_{15}H_{31}COOCH_3$, "Sigma-Aldrich," Saint Louis, MO, USA, ≥97%), *n*-octane ("Kriokhrom," Saint Petersburg, Russia, ≥99.5%) and *n*-dodecane ($C_{12}H_{26}$, "Acros Organics," New Jersey, NJ, USA, ≥99%).

3.2. Catalyst Preparation

Two sets of alumina-supported nickel phosphide catalysts with the nickel content about 7.5 wt% were prepared by the incipient wetness impregnation method from the phosphate- or phosphite-containing precursors with the subsequent temperature-programmed reduction.

Catalyst preparation from the phosphate-containing precursor (A). Support (γ-Al_2O_3) was incipiently impregnated with an aqueous solution of $(NH_4)_2HPO_4$ and $Ni(NO_3)_2$, followed by drying in air at room temperature overnight and at 110 °C for 3 h and then calcination at 500 °C in air for 3 h. The initial Ni/P molar ratio in precursor was 0.5. Then the oxide precursor was reduced with H_2 flow (100 mL/(min·g)) using the temperature program: heating to 370 °C at a ramp rate of 3 °C/min and then to 550, 600 or 650 °C at a ramp rate of 1 °C/min and keeping at the reduction temperature for 1 h. After reduction, the samples were passivated at room temperature for 2 h in 1 vol% O_2/He flow (40 mL/(min·g)) before taking out into the air for investigation by physicochemical methods. For the reactivity test, the catalysts were reduced in the catalytic reactor before experiments. The catalysts prepared from phosphate-containing precursor are denoted on the base of the precursor type (A) and the TPR temperature, for example, NiP_A/Al_2O_3(550) (shown in Table 1).

Catalyst preparation from the phosphite-containing precursor (I). The support (γ-Al_2O_3, SiO_2) was incipiently impregnated with an aqueous solution of $Ni(OH)_2$ and H_3PO_3 with consequent drying in air at room temperature overnight and at 80 °C for 24 h. The initial Ni/P molar ratio in precursor was 0.3. Dried precursors were reduced directly without calcination by TPR in H_2 flow (100 mL/(min·g)) using the following temperature program: heating to 550, 600 or 650 °C at a ramp rate of 1 °C/min and keeping at the reduction temperature for 1 h. The catalysts prepared from phosphite precursor are denoted on the base of the precursor type (I) and the TPR temperature, for example, NiP_I/Al_2O_3(550) (Table 1). For comparison, the reference silica-supported Ni_2P/SiO_2 catalyst (NiP_I/SiO_2(600)) was prepared by the same procedure.

3.3. Catalyst Characterization

The elemental analysis of the samples was conducted using inductively coupled plasma atomic emission spectroscopy (ICP-AES) on Optima 4300 DV (Perkin Elmer, France).

The textural properties of the catalysts were characterized using N_2 physisorption at 77 K with an ASAP 2400 instrument (Micromeritics, Norcross, GA, USA). The specific surface area (A_{BET}) was determined using a multipoint Brunauer-Emmett-Teller (BET) model. The average pore diameter (D_{pore}) and the pore size distribution were determined by the Barret-Joyner-Halenda (BJH) method using the desorption branch of the isotherm. The total pore volume (V_{pore}) was estimated at a relative pressure of 0.99.

The reduction peculiarities of the catalyst precursors were determined by the H_2 temperature-programmed reduction method (H_2-TPR). The calcined phosphate type precursor (or dried sample in the case of phosphite type precursor) in the amount of 0.10 g was loaded into a quartz U-tube reactor (5 mm in inner diameter) and pre-treated in argon atmosphere at 200 °C for 1 h. The experiments were carried out in 10 vol.% H_2/Ar flow (flow rate = 60 mL/min) at a heating rate of 10 °C/min in a temperature range from 80 to 900 °C. The H_2 consumption was evaluated using a thermal conductivity detector (TCD). A cold trap with a temperature of −60 °C mounted before the TCD was used to remove water from the exhaust gas.

X-ray diffraction (XRD) patterns were acquired on an X-ray diffractometer Bruker D8 Advance (Bruker, Germany) using CuK_α radiation (wavelength λ = 1.5418 Å) in 2θ scanning range from 10 to 70°. The qualitative phase analysis was performed using the JCPDS database [69]. The quantitative phase analysis and refining of the unit cell parameters were carried out by Rietveld analysis of a diffraction pattern using X'Pert High Score Plus software. The average crystallite size (D_{XRD}) was estimated using the Scherrer equation.

Transmission electron microscopy (TEM) images were obtained on a JEM-2010 instrument (JEOL, Tokyo, Japan) with an accelerating voltage of 200 kV and a resolution of 0.14 nm. To obtain statistical information, the structural parameters of ca. 250 particles were measured. The Sauter mean diameter was used to determine the mean particles diameter (D_s) by the Equation:

$$D_S = \frac{\sum n_i d_i^3}{\sum n_i d_i^2}, \quad (1)$$

where n_i is the number of particles, d_i is the diameter of the i^{th} particle.

NMR experiments were carried out using a Bruker Avance-400 spectrometer (Bruker, Germany) at the resonance frequencies of 104.31 and 161.923 MHz for ^{27}Al and ^{31}P nuclei respectively. Magic Angle Spinning (MAS) spectra were measured using a Bruker MAS NMR probe with 4-mm (outer diameter) ZrO_2 rotors at the spinning frequency of 14 kHz. The detailed procedure of ^{31}P MAS NMR measurements can be found in reference [27]. ^{27}Al MAS NMR spectra were measured at the same spinning frequency with a simple one-pulse sequence. We used a short non-selective π/8 pulse of 0.5 μs with a 500 ms second repetition delay; 512 transients were recorded for each sample. The spectra were referenced to 0.1 mM $Al[H_2O]_6^{3+}$ solution. Deconvolution of ^{27}Al NMR spectra was carried out in Dmfit program [70] using Simple Czjzek model that accounts for Gaussian quadrupole parameters distribution in disordered solids [65]. To avoid oxidation of reduced catalysts by air, all samples were sealed in glass ampoules without oxygen access. Prior to NMR experiments, the catalysts were transferred from ampoule to NMR rotor in a glove box under argon atmosphere. This technique helps to minimize possible oxidation during NMR spectra acquisition.

The acidic properties of the catalysts were characterized by temperature-programmed desorption of ammonia (NH_3-TPD) using an Autosorb-1 apparatus (Quantachrome Instruments, Boynton Beach, FL, USA). Prior to ammonia adsorption, the precursor sample (0.25 g) was reduced at the given reduction temperature (550–650 °C) for 1 hour in hydrogen flow (25 mL/min) and then cooled to 120 °C. Subsequently, the sample was saturated with NH_3 for 30 min. The physically adsorbed ammonia was desorbed from the sample with He flow (25 mL/min) at 120 °C for 30 min. Desorption of ammonia was started by increasing the temperature from 120 °C up to 600 °C at a heating rate of 10 °C/min. The desorbed NH_3 was detected by a TCD.

3.4. Catalytic Activity Measurements

The reaction of methyl palmitate HDO was performed in a high-pressure fixed-bed reactor (inner diameter 9 mm and total length 265 mm) at the temperature range of 250–330 °C, hydrogen pressure 3.0 MPa, H_2/feed volume ratio 600 Nm^3/m^3 and methyl palmitate LHSV in the range of 2.4–12 h^{-1} ((cm^3 of MP)/(cm^3 of catalysts) per hour). The composition of the reaction mixture amounted to methyl palmitate – 10 wt% (oxygen content – 1.183 wt%), *n*-octane (used as internal standard for quantification of liquid product) – 0.5 wt% and the rest – *n*-dodecane. For catalytic activity measurements, 0.5 cm^3 of the catalyst precursor was diluted with silicon carbide (0.2–0.3 mm) in a ratio of 1:9 and placed in the reactor between two layers of SiC. Then the sample of the precursor was reduced as described in Section 3.2. The liquid reaction products were collected every hour till steady-state condition and time on stream was not less than 8 h for each stage.

The conversion of methyl palmitate (X_{MP}), conversion of oxygen-containing compounds (X_O) and the selectivity to C_{16} hydrocarbons (S_{C16}) were calculated according to Equations:

$$X_{MP} = \left(1 - \frac{n_{MP}}{n^o_{MP}}\right) \times 100, \% \quad (2)$$

$$X_O = \left(1 - \frac{n_O}{n^o_O}\right) \times 100, \% \quad (3)$$

$$S_{C16} = \left(\frac{n_{C16}}{n^o_{MP} - n_{MP}}\right) \times 100, \% \quad (4)$$

where $n^o{}_{MP}$ and n_{MP} are the initial and the current methyl palmitate content (mol/L), $n^o{}_O$ and n_O are the initial and current oxygen content (mol/L), n_{C16} is the concentration of C_{16} hydrocarbons (mol/L) in the reaction mixture at X_{MP} = 100%. The relative error in determining of the methyl palmitate (from GC data) and oxygen-containing compounds (from elemental analysis by Vario EL Cube) conversions was no more than 1%.

3.5. Product Analysis

The reaction products were identified using a GC-MS technique (Agilent Technologies 6890N with MSD 5973, Santa Clara, CA, USA) with a VF-5MS quartz capillary column (30 m × 0.25 mm × 0.25 μm). The liquid samples were analysed with a gas chromatography system (Agilent 6890N, Santa Clara, CA, USA) equipped with HP-1MS column (30 m × 0.32 mm × 1.0 μm) and flame ionization detector (FID). Gaseous phase products were analysed online with a gas chromatograph (Chromos 1000, Dzerzhinsk, Russia) equipped with a column packed with 80/100 mesh HayeSep®(Sigma-Aldrich, Saint Louis, MO, USA) and FID. The concentrations of CO and CO_2 were analysed in the form of methane after methanation over reduced Pd catalyst at 340 °C. The carbon balance across the reactor for all experiments was not less than 95%.

The total oxygen content in the reaction mixtures was evaluated using CHNSO elemental analyser Vario EL Cube (Elementar Analysensysteme GmbH, Hanau, Germany). The method is based on high-temperature pyrolysis of a liquid sample of the reaction mixture in a reducing atmosphere at 1170 °C and the resulting oxygen-containing radicals interact quantitatively with the carbon filler to form carbon monoxide (Boudouard equilibrium). An IR detector was used to quantify the CO.

4. Conclusions

Effect of precursors on the physicochemical and catalytic properties of alumina-supported nickel phosphide catalysts differing in precursors was studied. $Ni(NO_3)_2$ and $(NH_4)_2HPO_4$ (phosphate precursor, NiP_A/Al_2O_3 catalyst) or $Ni(OH)_2$ and H_3PO_3 (phosphite precursor, NiP_I/Al_2O_3 catalyst) pairs of nickel and phosphorus compounds were used for catalyst preparation by temperature-programmed reduction. It was found that NiP_I precursor is reduced at lower temperatures apparently due to nickel phosphite and H_3PO_3 disproportionation with the formation of PH_3 interacting readily with nickel species and producing Ni_2P nanoparticles in the temperature range of 550–650 °C. On the other hand, starting from phosphate precursor, we did not succeed in the production of Ni_2P and the reduction at the temperature as high as 650 °C gives the mixture of Ni_3P and $Ni_{12}P_5$ phases. Using ^{31}P and ^{27}Al MAS NMR, the formation of aluminium phosphates in all catalysts was revealed. Interaction of phosphate groups with alumina surface hinders the formation of the desired Ni_2P phase and leads to an irreversible change in textural characteristics and surface properties of γ-Al_2O_3. Indeed, the increase in the number of weak acid sites, which are usually associated with Brønsted acidity, has been observed by means of NH_3-TPD in the supported catalysts in comparison with the alumina support. NiP_I/Al_2O_3 catalyst displays significantly higher activity in methyl palmitate HDO compared to the NiP_A/Al_2O_3 sample within the temperature region of

250–330 °C that is in agreement with the literature data reported the superiority of Ni_2P phase against $Ni_3P/Ni_{12}P_5$ systems in HDO of aliphatic esters over silica-supported nickel phosphide catalysts.

The performances of alumina- and silica-supported Ni_2P catalysts were compared in methyl palmitate HDO using NiP_I/Al_2O_3 and NiP_I/SiO_2 catalysts with nearly the same nickel content and mean particle size. The employment of alumina instead of silica for Ni_2P supporting allows a significant increase of the methyl palmitate conversion. Considering the tentative scheme of methyl palmitate transformation and reaction products distribution over NiP_I/Al_2O_3 and NiP_I/SiO_2 catalysts, we conclude that the acceleration of methyl palmitate hydrolysis over acid sites of the alumina-supported catalyst is the reason of increased activity of NiP_I/Al_2O_3 catalyst.

In general, the proper balance between metal and acid sites provides the superior performance of the NiP_I/Al_2O_3 catalyst in the complicated scheme of methyl palmitate transformation, which includes the framework of acid- and metal-catalysed reactions.

Supplementary Materials: The following are available online at http://www.mdpi.com/2073-4344/8/11/515/s1, Figure S1: Pore size distributions determined from the desorption branch of N_2 isotherm for (a) NiP_A/Al_2O_3 and (b) NiP_I/Al_2O_3 catalysts reduced at 550, 600 and 650 °C as well as for Al_2O_3 support. Figure S2: XRD patterns of NiP_I/SiO_2(600) catalyst prepared from phosphite precursor and reduced at temperature of 600 °C and SiO_2 support. Figure S3: TEM images of Ni_xP_y/γ-Al_2O_3 catalysts prepared from different precursors: (a) NiP_A/Al_2O_3 650 and (b) NiP_I/Al_2O_3 600. Figure S4: Full-scale mass-normalized 14 kHz MAS ^{31}P spectra of NiP_I/Al_2O_3 reduced at 550, 600 and 650 °C. A significant decrease in intensity of the line corresponding to PO_x groups can be observed for the sample reduced at 650 °C. Figure S5: Temperature effect on the conversion of methyl palmitate and oxygen-containing compounds over NiP_A/Al_2O_3 650 and NiP_I/Al_2O_3 600 catalysts. Figure S6: Conversions of methyl laurate, lauric acid, dodecanal and dodecanol over Ni_2P/SiO_2 catalyst. Figure S7: MP conversion and total oxygen-containing compounds conversion as a function of time on stream for Ni_2P/Al_2O_3 and Ni_2P/SiO_2 catalysts. Figure S8: Dependence of the CO and CO_2 sum from pentadecane content in methyl palmitate hydrodeoxygenation over NiP_A/Al_2O_3 650 catalysts.

Author Contributions: G.A.B. conceived and designed the experiments and supervised the work; I.V.D. and I.V.S. performed the catalyst synthesis; I.V.D., I.V.S. and P.V.A. performed the catalytic activity tests; E.Y.G. performed the catalyst characterization by TEM; V.P.P. performed the catalyst characterization by XRD; E.G.K. performed the catalyst characterization by NH_3-TPD; I.V.Y. and O.B.L. performed the catalyst characterization by MAS NMR; I.V.D., P.V.A. and G.A.B. analysed the experimental data and wrote the paper.

Funding: This work was conducted within the framework of the budget project No. AAAA-A17-117041710075-0 for Boreskov Institute of Catalysis.

Acknowledgments: The authors are grateful to V.A. Rogov for catalysts characterization by H_2-TPR, A.V. Ishchenko for catalysts characterization by TEM and S.A. Prikhod'ko for reaction products identification using GC/MS technique.

Conflicts of Interest: The authors declare no conflict of interest.

References

1. Maity, S.K. Opportunities, recent trends and challenges of integrated biorefinery: Part II. *Renew. Sustain. Energy Rev.* **2015**, *43*, 1446–1466. [CrossRef]
2. Arun, N.; Sharma, R.V.; Dalai, A.K. Green diesel synthesis by hydrodeoxygenation of bio-based feedstocks: Strategies for catalyst design and development. *Renew. Sustain. Energy Rev.* **2015**, *48*, 240–255. [CrossRef]
3. Li, X.; Luo, X.Y.; Jin, Y.B.; Li, J.Y.; Zhang, H.D.; Zhang, A.P.; Xie, J. Heterogeneous sulfur-free hydrodeoxygenation catalysts for selectively upgrading the renewable bio-oils to second generation biofuels. *Renew. Sustain. Energy Rev.* **2018**, *82*, 3762–3797. [CrossRef]
4. Ameen, M.; Azizan, M.T.; Yusup, S.; Ramli, A.; Yasir, M. Catalytic hydrodeoxygenation of triglycerides: An approach to clean diesel fuel production. *Renew. Sustain. Energy Rev.* **2017**, *80*, 1072–1088. [CrossRef]
5. Mohammad, M.; Hari, T.K.; Yaakob, Z.; Sharma, Y.C.; Sopian, K. Overview on the production of paraffin based-biofuels via catalytic hydrodeoxygenation. *Renew. Sustain. Energy Rev.* **2013**, *22*, 121–132. [CrossRef]
6. Bezergianni, S.; Dimitriadis, A. Comparison between different types of renewable diesel. *Renew. Sustain. Energy Rev.* **2013**, *21*, 110–116. [CrossRef]
7. Lapuerta, M.; Villajos, M.; Agudelo, J.R.; Boehman, A.L. Key properties and blending strategies of hydrotreated vegetable oil as biofuel for diesel engines. *Fuel Process. Technol.* **2011**, *92*, 2406–2411. [CrossRef]

8. Singh, D.; Subramanian, K.A.; Garg, M.O. Comprehensive review of combustion, performance and emissions characteristics of a compression ignition engine fueled with hydroprocessed renewable diesel. *Renew. Sustain. Energy Rev.* **2018**, *81*, 2947–2954. [CrossRef]
9. Ryymin, E.M.; Honkela, M.L.; Viljava, T.R.; Krause, A.O.I. Insight to sulfur species in the hydrodeoxygenation of aliphatic esters over sulfided NiMo/γ-Al_2O_3 catalyst. *Appl. Catal. A Gen.* **2009**, *358*, 42–48. [CrossRef]
10. Kubicka, D.; Horacek, J. Deactivation of HDS catalysts in deoxygenation of vegetable oils. *Appl. Catal. A Gen.* **2011**, *394*, 9–17. [CrossRef]
11. Deliy, I.V.; Vlasova, E.N.; Nuzhdin, A.L.; Gerasimov, E.Y.; Bukhtiyarova, G.A. Hydrodeoxygenation of methyl palmitate over sulfided Mo/Al_2O_3, CoMo/Al_2O_3 and NiMo/Al_2O_3 catalysts. *RSC Adv.* **2014**, *4*, 2242–2250. [CrossRef]
12. Laurent, E.; Delmon, B. Influence of Water in the Deactivation of a Sulfided NiMo γ-Al_2O_3 Catalyst during Hydrodeoxygenation. *J. Catal.* **1994**, *146*, 281–291. [CrossRef]
13. Pelardy, F.; Daudin, A.; Devers, E.; Dupont, C.; Raybaud, P.; Brunet, S. Deep HDS of FCC gasoline over alumina supported CoMoS catalyst: Inhibiting effects of carbon monoxide and water. *Appl. Catal. B Environ.* **2016**, *183*, 317–327. [CrossRef]
14. Deliy, I.V.; Vlasova, E.N.; Aleksandrov, P.V.; Aleshina, G.I.; Bukhtiyarov, V.I.; Gerasimov, E.Y.; Nuzhdin, A.L.; Bukhtiyarova, G.A. Inhibition of SRGO Hydrodesulfurization over CoMo/Al_2O_3 Catalyst: Comparison of Rapeseed Oil and Carbon Monoxide Effects. *Int. J. Environ. Sci.* **2017**, *2*, 386–391.
15. Alvarez-Galvan, M.C.; Blanco-Brieva, G.; Capel-Sanchez, M.; Morales-DelaRosa, S.; Campos-Martin, J.M.; Fierro, J.L.G. Metal phosphide catalysts for the hydrotreatment of non-edible vegetable oils. *Catal. Today* **2018**, *302*, 242–249. [CrossRef]
16. Kordulis, C.; Bourikas, K.; Gousi, M.; Kordouli, E.; Lycourghiotis, A. Development of nickel based catalysts for the transformation of natural triglycerides and related compounds into green diesel: A critical review. *Appl. Catal. B Environ.* **2016**, *181*, 156–196. [CrossRef]
17. Chen, J.X.; Shi, H.; Li, L.; Li, K.L. Deoxygenation of methyl laurate as a model compound to hydrocarbons on transition metal phosphide catalysts. *Appl. Catal. B Environ.* **2014**, *144*, 870–884. [CrossRef]
18. Yang, Y.X.; Ochoa-Hernandez, C.; O'Shea, V.A.D.; Coronado, J.M.; Serrano, D.P. Ni_2P/SBA-15 As a Hydrodeoxygenation Catalyst with Enhanced Selectivity for the Conversion of Methyl Oleate Into n-Octadecane. *ACS Catal.* **2012**, *2*, 592–598. [CrossRef]
19. Yang, Y.; Chen, J.X.; Shi, H. Deoxygenation of Methyl Laurate as a Model Compound to Hydrocarbons on Ni_2P/SiO_2, Ni_2P/MCM-41, and Ni_2P/SBA-15 Catalysts with Different Dispersions. *Energy Fuels* **2013**, *27*, 3400–3409. [CrossRef]
20. Yang, Y.X.; Ochoa-Hernandez, C.; Pizarro, P.; O'Shea, V.A.D.; Coronado, J.M.; Serrano, D.P. Influence of the Ni/P ratio and metal loading on the performance of Ni_xP_y/SBA-15 catalysts for the hydrodeoxygenation of methyl oleate. *Fuel* **2015**, *144*, 60–70. [CrossRef]
21. Xue, Y.A.; Guan, Q.X.; Li, W. Synthesis of bulk and supported nickel phosphide using microwave radiation for hydrodeoxygenation of methyl palmitate. *RSC Adv.* **2015**, *5*, 53623–53628. [CrossRef]
22. Shi, H.; Chen, J.X.; Yang, Y.; Tian, S.S. Catalytic deoxygenation of methyl laurate as a model compound to hydrocarbons on nickel phosphide catalysts: Remarkable support effect. *Fuel Process. Technol.* **2014**, *118*, 161–170. [CrossRef]
23. Guan, Q.X.; Han, F.; Li, W. Catalytic performance and deoxygenation path of methyl palmitate on Ni_2P/SiO_2 synthesized using the thermal decomposition of nickel hypophosphite. *RSC Adv.* **2016**, *6*, 31308–31315. [CrossRef]
24. Guan, Q.X.; Wan, F.F.; Han, F.; Liu, Z.H.; Li, W. Hydrodeoxygenation of methyl palmitate over MCM-41 supported nickel phosphide catalysts. *Catal. Today* **2016**, *259*, 467–473. [CrossRef]
25. Shamanaev, I.V.; Deliy, I.V.; Pakharukova, V.P.; Gerasimov, E.Y.; Rogov, V.A.; Bukhtiyarova, G.A. Effect of the preparation conditions on the physicochemical and catalytic properties of Ni_2P/SiO_2 catalysts. *Russ. Chem. Bull.* **2015**, *64*, 2361–2370. [CrossRef]
26. Shamanaev, I.V.; Deliy, I.V.; Aleksandrov, P.V.; Gerasimov, E.Y.; Pakharukova, V.P.; Kodenev, E.G.; Ayupov, A.B.; Andreev, A.S.; Lapina, O.B.; Bukhtiyarova, G.A. Effect of precursor on the catalytic properties of Ni_2P/SiO_2 in methyl palmitate hydrodeoxygenation. *RSC Adv.* **2016**, *6*, 30372–30383. [CrossRef]

27. Deliy, I.V.; Shamanaev, I.V.; Gerasimov, E.Y.; Pakharukova, V.P.; Yakovlev, I.V.; Lapina, O.B.; Aleksandrov, P.V.; Bukhtiyarova, G.A. HDO of Methyl Palmitate over Silica-Supported Ni Phosphides: Insight into Ni/P Effect. *Catalysts* **2017**, *7*, 298. [CrossRef]
28. Chen, J.X.; Han, M.M.; Zhao, S.; Pan, Z.Y.; Zhang, Z.N. An in situ approach to preparing Ni_2P/SiO_2 catalyst under mild conditions and its performance for the deoxygenation of methyl laurate to hydrocarbons. *Catal. Sci. Technol.* **2016**, *6*, 3938–3949. [CrossRef]
29. Chen, J.X.; Yang, Y.; Shi, H.; Li, M.F.; Chu, Y.; Pan, Z.Y.; Yu, X.B. Regulating product distribution in deoxygenation of methyl laurate on silica-supported Ni-Mo phosphides: Effect of Ni/Mo ratio. *Fuel* **2014**, *129*, 1–10. [CrossRef]
30. Pan, Z.Y.; Wang, R.J.; Li, M.F.; Chu, Y.; Chen, J.X. Deoxygenation of methyl laurate to hydrocarbons on silica-supported Ni-Mo phosphides: Effect of calcination temperatures of precursor. *J. Energy Chem.* **2015**, *24*, 77–86. [CrossRef]
31. Shamanaev, I.V.; Deliy, I.V.; Gerasimov, E.Y.; Pakharukova, V.P.; Kodenev, E.G.; Aleksandrov, P.V.; Bukhtiyarova, G.A. Synergetic Effect of Ni_2P/SiO_2 and γ-Al_2O_3 Physical Mixture in Hydrodeoxygenation of Methyl Palmitate. *Catalysts* **2017**, *7*, 329. [CrossRef]
32. Laurent, E.; Delmon, B. Study of the Hydrodeoxygenation of Carbonyl, Carboxylic and Guaiacyl Groups over Sulfided CoMo/γ-Al_2O_3 and NiMo/γ-Al_2O_3 Catalyst.2. Influence of Water, Ammonia and Hydrogen-Sulfide. *Appl. Catal. A Gen.* **1994**, *109*, 97–115. [CrossRef]
33. Senol, O.I.; Viljava, T.R.; Krause, A.O.I. Hydrodeoxygenation of methyl esters on sulphided NiMo/γ-Al_2O_3 and CoMo/γ-Al_2O_3 catalysts. *Catal. Today* **2005**, *100*, 331–335. [CrossRef]
34. Mehrabadi, B.A.T.; Eskandari, S.; Khan, U.; White, R.D.; Regalbuto, J.R. A Review of Preparation Methods for Supported Metal Catalysts. *Adv. In Catal.* **2017**, *61*, 1–35. [CrossRef]
35. Coumans, A.E.; Hensen, E.J.M. A real support effect on the hydrodeoxygenation of methyl oleate by sulfided NiMo catalysts. *Catal. Today* **2017**, *298*, 181–189. [CrossRef]
36. Bukhtiyarova, G.A.; Mart'yanov, O.N.; Yakushkin, S.S.; Shuvaeva, M.A.; Bayukov, O.A. State of iron in nanoparticles prepared by impregnation of silica gel and aluminum oxide with $FeSO_4$ solutions. *Phys. Solid State* **2010**, *52*, 826–837. [CrossRef]
37. Zhang, Z.N.; Tang, M.X.; Chen, J.X. Effects of P/Ni ratio and Ni content on performance of γ-Al_2O_3-supported nickel phosphides for deoxygenation of methyl laurate to hydrocarbons. *Appl. Surf. Sci.* **2016**, *360*, 353–364. [CrossRef]
38. Winoto, H.P.; Ahn, B.S.; Jae, J. Production of gamma-valerolactone from furfural by a single-step process using Sn-Al-Beta zeolites: Optimizing the catalyst acid properties and process conditions. *J. Ind. Eng. Chem.* **2016**, *40*, 62–71. [CrossRef]
39. Motokura, K. Synergistic Catalysis by Multifunctionalized Solid Surfaces for Nucleophilic Addition Reactions. *J. Jpn. Petrol. Inst.* **2014**, *57*, 95–108. [CrossRef]
40. Peroni, M.; Mancino, G.; Barath, E.; Gutierrez, O.Y.; Lercher, J.A. Bulk and γ-Al_2O_3-supported Ni_2P and MoP for hydrodeoxygenation of palmitic acid. *Appl. Catal. B Environ.* **2016**, *180*, 301–311. [CrossRef]
41. Cecilia, J.A.; Jimenez-Morales, I.; Infantes-Molina, A.; Rodriguez-Castellon, E.; Jimenez-Lopez, A. Influence of the silica support on the activity of Ni and Ni_2P based catalysts in the hydrodechlorination of chlorobenzene. Study of factors governing catalyst deactivation. *J. Mol. Catal. A Chem.* **2013**, *368*, 78–87. [CrossRef]
42. Chen, J.X.; Zhou, S.J.; Ci, D.H.; Zhang, J.X.; Wang, R.J.; Zhang, J.Y. Influence of Supports on Structure and Performance of Nickel Phosphide Catalysts for Hydrodechlorination of Chlorobenzene. *Ind. Eng. Chem. Res.* **2009**, *48*, 3812–3819. [CrossRef]
43. Sawhill, S.J.; Layman, K.A.; Van Wyk, D.R.; Engelhard, M.H.; Wang, C.; Bussell, M.E. Thiophene hydrodesulfurization over nickel phosphide catalysts: Effect of the precursor composition and support. *J. Catal.* **2005**, *231*, 300–313. [CrossRef]
44. Wu, S.K.; Lai, P.C.; Lin, Y.C.; Wan, H.P.; Lee, H.T.; Chang, Y.H. Atmospheric Hydrodeoxygenation of Guaiacol over Alumina-, Zirconia-, and Silica-Supported Nickel Phosphide Catalysts. *ACS Sustain. Chem. Eng.* **2013**, *1*, 349–358. [CrossRef]
45. Wu, S.K.; Lai, P.C.; Lin, Y.C. Atmospheric Hydrodeoxygenation of Guaiacol over Nickel Phosphide Catalysts: Effect of Phosphorus Composition. *Catal. Lett.* **2014**, *144*, 878–889. [CrossRef]
46. Stinner, C.; Tang, Z.; Haouas, M.; Weber, T.; Prins, R. Preparation and 31P NMR characterization of nickel phosphides on silica. *J. Catal.* **2002**, *208*, 456–466. [CrossRef]

47. Oyama, S.; Wang, X.; Lee, Y.; Bando, K.; Requejo, F. Effect of phosphorus content in nickel phosphide catalysts studied by XAFS and other techniques. *J. Catal.* **2002**, *210*, 207–217. [CrossRef]
48. Li, K.L.; Wang, R.J.; Chen, J.X. Hydrodeoxygenation of Anisole over Silica-Supported Ni_2P, MoP, and NiMoP Catalysts. *Energy Fuels* **2011**, *25*, 854–863. [CrossRef]
49. Oyama, S.; Lee, Y. The active site of nickel phosphide catalysts for the hydrodesulfurization of 4,6-DMDBT. *J. Catal.* **2008**, *258*, 393–400. [CrossRef]
50. Clark, P.A.; Oyama, S.T. Alumina-supported molybdenum phosphide hydroprocessing catalysts. *J. Catal.* **2003**, *218*, 78–87. [CrossRef]
51. Li, L.L.; Han, C.X.; Han, X.Y.; Zhou, Y.X.; Yang, L.; Zhang, B.G.; Hu, J.L. Catalytic Decomposition of Toxic Chemicals over Metal-Promoted Carbon Nanotubes. *Environ. Sci. Technol.* **2011**, *45*, 726–731. [CrossRef] [PubMed]
52. Song, L.M.; Zhang, S.J.; Wei, Q.W. A new route for synthesizing nickel phosphide catalysts with high hydrodesulfurization activity based on sodium dihydrogenphosphite. *Catal. Commun.* **2011**, *12*, 1157–1160. [CrossRef]
53. Yang, S.F.; Prins, R. New synthesis method for nickel phosphide hydrotreating catalysts. *Chem. Commun.* **2005**, 4178–4180. [CrossRef] [PubMed]
54. Montesinos-Castellanos, A.; Zepeda, T.A.; Pawelec, B.; Fierro, J.L.G.; de los Reyes, J.A. Preparation, characterization, and performance of alumina-supported nanostructured Mo-phosphide systems. *Chem. Mater.* **2007**, *19*, 5627–5636. [CrossRef]
55. Quartararo, J.; Amoureux, J.P.; Grimblot, J. Sol-gel synthesis, characterization by solid state NMR and HDS activity of Mo-alumina and Mo-P-alumina based catalysts. *J. Mol. Catal. A Chem.* **2000**, *162*, 353–365. [CrossRef]
56. Fitz, C.W.; Rase, H.F. Effects of Phosphorus on Nickel Molybdenum Hydrodesulfurization Hydrodenitrogenation Catalysts of Varying Metals Content. *Ind. Eng. Chem. Prod. Res. Dev.* **1983**, *22*, 40–44. [CrossRef]
57. Berteau, P.; Delmon, B. Modified Aluminas - Relationship between Activity in 1-Butanol Dehydration and Acidity Measured by NH_3 TPD. *Catal. Today* **1989**, *5*, 121–137. [CrossRef]
58. Lee, Y.K.; Oyama, S.T. Bifunctional nature of a SiO_2-supported Ni_2P catalyst for hydrotreating: EXAFS and FTIR studies. *J. Catal.* **2006**, *239*, 376–389. [CrossRef]
59. Chen, J.X.; Guo, T.; Li, K.L.; Sun, L.M. A facile approach to enhancing activity of Ni_2P/SiO_2 catalyst for hydrodechlorination of chlorobenzene: Promoting effect of water and oxygen. *Catal. Sci. Technol.* **2015**, *5*, 2670–2680. [CrossRef]
60. Krawietz, T.R.; Lin, P.; Lotterhos, K.E.; Torres, P.D.; Barich, D.H.; Clearfield, A.; Haw, J.F. Solid phosphoric acid catalyst: A multinuclear NMR and theoretical study. *J. Am. Chem. Soc.* **1998**, *120*, 8502–8511. [CrossRef]
61. Eichele, K.; Wasylishen, R.E. P-31-NMR Study of Powder and Single-Crystal Samples of Ammonium Dihydrogen Phosphate - Effect of Homonuclear Dipolar Coupling. *J. Phys. Chem.-US* **1994**, *98*, 3108–3113. [CrossRef]
62. Koranyi, T.I.; Vit, Z.; Nagy, J.B. Support and pretreatment effects on the hydrotreating activity of SBA-15 and CMK-5 supported nickel phosphide catalysts. *Catal. Today* **2008**, *130*, 80–85. [CrossRef]
63. Bekaert, E.; Bernardi, J.; Boyanov, S.; Monconduit, L.; Doublet, M.L.; Menetrier, M. Direct Correlation between the 31P MAS NMR Response and the Electronic Structure of Some Transition Metal Phosphides. *J. Phys. Chem. C* **2008**, *112*, 20481–20490. [CrossRef]
64. Quartararo, J.; Guelton, M.; Rigole, M.; Amoureux, J.P.; Fernandez, C.; Grimblot, J. Sol-gel synthesis of alumina modified by phosphorus: A solid state NMR characterization study. *J. Mater. Chem.* **1999**, *9*, 2637–2646. [CrossRef]
65. d'Espinose de la Caillerie, J.B.; Fretigny, C.; Massiot, D. MAS NMR spectra of quadrupolar nuclei in disordered solids: The Czjzek model. *J. Magn. Reson.* **2008**, *192*, 244–251. [CrossRef] [PubMed]
66. Oyama, S.T.; Gott, T.; Zhao, H.Y.; Lee, Y.K. Transition metal phosphide hydroprocessing catalysts: A review. *Catal. Today* **2009**, *143*, 94–107. [CrossRef]
67. Rodriguez, J.A.; Vines, F.; Liu, P.; Illas, F. Role of C and P Sites on the Chemical Activity of Metal Carbides and Phosphides: From Clusters to Single-Crystal Surfaces. *Model Syst. Catal.* **2010**, 117–132. [CrossRef]
68. Zhao, X.H.; Wei, L.; Cheng, S.Y.; Julson, J. Review of Heterogeneous Catalysts for Catalytically Upgrading Vegetable Oils into Hydrocarbon Biofuels. *Catalysts* **2017**, *7*, 83. [CrossRef]

69. *International Centre for Diffraction Data*; JCPDS: Swarthmore, PA, USA, 1997.
70. Massiot, D.; Fayon, F.; Capron, M.; King, I.; Le Calve, S.; Alonso, B.; Durand, J.O.; Bujoli, B.; Gan, Z.H.; Hoatson, G. Modelling one- and two-dimensional solid-state NMR spectra. *Magn. Reson. Chem.* **2002**, *40*, 70–76. [CrossRef]